Title

Circumvention of luteolysis reveals parturition pathways in mice dependent upon innate type 2 immunity.

Journal

Immunity, 56(3)

Authors

Siewiera, Johan
McIntyre, Tara
Cautivo, Kelly
et al.

Publication Date

2023-03-14

DOI

10.1016/j.immuni.2023.01.005

Peer reviewed

HHS Public Access

Author manuscript

Immunity. Author manuscript; available in PMC 2024 March 14.

Published in final edited form as:

Immunity. 2023 March 14; 56(3): 606–619.e7. doi:10.1016/j.immuni.2023.01.005.

Circumvention of luteolysis reveals parturition pathways in mice dependent upon innate type 2 immunity

Johan Siewiera[1], **Tara I. McIntyre**[2], **Kelly M. Cautivo**[1], **Karim Mahiddine**[1], **Damon Rideaux**[1], **Ari B. Molofsky**[1,2,3], **Adrian Erlebacher**[1,2,3,4,*]

[1]Department of Laboratory Medicine, University of California San Francisco, San Francisco, California 94143, USA.

[2]Biomedical Sciences Program, University of California San Francisco, San Francisco, California 94143, USA.

[3]Bakar ImmunoX Initiative, University of California San Francisco, San Francisco, California 94143, USA.

[4]Center for Reproductive Sciences, University of California San Francisco, San Francisco, California 94143, USA.

SUMMARY

Although mice normally enter labor when their ovaries stop producing progesterone (luteolysis), parturition can also be triggered in this species through uterus-intrinsic pathways potentially analogous to the ones that trigger parturition in humans. Such pathways, however, remain largely undefined in both species. Here, we report that mice deficient in innate type 2 immunity experienced profound parturition delays when manipulated endocrinologically to circumvent luteolysis, thus obliging them to enter labor through uterus-intrinsic pathways. We found that these pathways were in part driven by the alarmin IL-33 produced uterine interstitial fibroblasts. We also implicated important roles for uterine group 2 innate lymphoid cells, which demonstrated IL-33-dependent activation prior to labor onset, and eosinophils, which displayed evidence of elevated turnover in the prepartum uterus. These findings reveal a role for innate type 2 immunity in controlling the timing of labor onset through a cascade potentially relevant to human parturition.

Corresponding author/lead contact: adrian.erlebacher@ucsf.edu.
*Lead contact: Adrian Erlebacher

AUTHOR CONTRIBUTIONS

J.S., T.I.M., K.M.C., K.M., and D.R. performed experiments. J.S., A.B.M, and A.E. designed experiments. J.S. and A.E. analyzed data and wrote and edited the manuscript. A.B.M. and T.I. M. edited the manuscript. A.E. conceived of the project and supervised the research.

DECLARATION OF INTERESTS

The authors declare no competing interests.

INCLUSION AND DIVERSITY

One or more of the authors of this paper self-identifies as an underrepresented ethnic minority in science. One or more of the authors of this paper self-identifies as a member of the LGBTQIA+ community.

Graphical Abstract

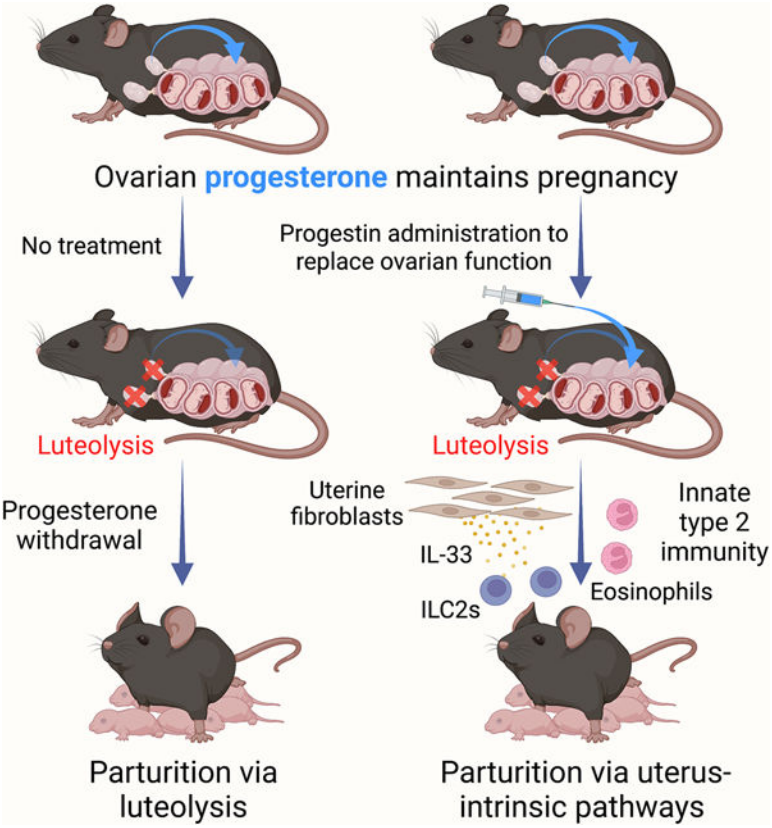

eTOC Blurb

Divergence across species in the endocrine control of labor onset has hindered our understanding of parturition mechanisms. Siewiera et al. uncover a parturition-promoting role for innate type 2 immunity in mice when they are manipulated endocrinologically to resemble humans.

INTRODUCTION

Parturition, i.e., the act of giving birth, is the end result of a process that transforms the late gestation gravid uterus into the highly contractile tissue that expels the conceptus (for reviews, see[1,2]). In humans, this process is thought to be mediated through a core set of uterus-intrinsic pathways that operate under the influence of endocrine, mechanical, and fetus-derived signals. The nature of these pathways is poorly understood, however, a knowledge gap that exemplifies the lack of insight into parturition mechanisms across species[1]. In turn, this deficit has hindered the development of rational therapies for preterm labor, a highly prevalent obstetrical complication and major cause of neonatal morbidity and mortality[3].

A major difficulty in elucidating parturition mechanisms with human relevance is the high degree of divergence across species in the endocrine control of labor onset[1]. Pregnancy requires the maintenance of high plasma progesterone (P4) concentrations, and primates

enter labor while these concentrations remain elevated, highlighting these species' reliance on uterus-intrinsic parturition pathways. In contrast, parturition onset in mice, the species of choice for mechanistic dissection, is triggered when the ovary starts expressing the P4-metabolizing enzyme 20α-hydroxysteroid dehydrogenase (20α-HSD). This process, known as luteolysis, leads to a systemic drop in P4 concentrations and consequent rapid maturation of the myometrium, the smooth muscle layer of the uterus. However, sidelining the effects of luteolysis through exogenous P4 administration extends gestation length only ~2 days[4,5], suggesting that mice also bear uterus-intrinsic parturition pathways. Indeed, the peri-partum uterus of both mice and humans show evidence of low-grade, sterile inflammation, which has led to the suggestion that immune activation contributes to parturition in both species[6,7]. To date, work on mouse parturition has not addressed these P4-independent, uterus-intrinsic parturition pathways but rather the pathways that induce luteolysis[8].

Previously, we identified *Il33*, which encodes the cytokine interleukin-33 (IL-33), as one of ~800 genes in mice subject to active, transcriptional silencing in the stromal cells of the early gestation decidua, the specialized endometrial tissue that surrounds the conceptus and that separates it from the myometrium[4]. IL-33 is an IL-1 superfamily member that functions as a pro-inflammatory alarmin and potent driver of type 2 immunity when released by tissue damage from its nucleus-sequestered state, with many of its effects mediated through group 2 innate lymphoid cells (ILC2s) and eosinophils[9]. Thus, given that placental growth and development disrupts the integrity of neighboring decidual tissue, *Il33* silencing appeared as a feature of the maternal-fetal interface that could limit maladaptive inflammatory reactions. However, we also found that *Il33* expression is maintained in the myometrium, suggesting a potential requirement for IL-33 activity in this tissue layer. Indeed, IL-33 has been implicated in the sensitization of smooth muscle cells (SMCs) to pro-contractile signals and is thought to contribute to a diverse set of pathologic and infectious processes that involve SMC contraction[10].

Here, we present evidence that IL-33, ILC2s, and eosinophils play key roles in the control of on time labor onset in mice. These roles are not apparent when parturition is governed by luteolysis, but instead when we artificially maintain high circulating P4 concentrations to create an experimental model that obliges labor to be initiated by uterus-intrinsic pathways, as it does in humans. We also map the source of IL-33 to platelet-derived growth factor receptor α-(PDGFRα-) expressing interstitial uterine fibroblasts and reveal activation of the type 2 immune axis in the uterus immediately prior to labor onset. These observations provide a foundation for dissecting further upstream and downstream components of a labor-inducing cascade potentially relevant to human parturition.

RESULTS

IL-33 is required for on-time parturition when only uterus-intrinsic pathways are available to drive labor onset.

To evaluate the role of IL-33 in mouse parturition, we first assessed whether IL-33 deficiency affected P4 metabolism systemically given that changes in plasma P4 concentrations alone can influence parturition timing. In addition, injection of supplemental P4 or its more potent analog medroxyprogesterone acetate[11] (MPA) was the means by

which we sidelined ovarian control over labor onset and obliged it instead to commence through uterus-intrinsic pathways. When left untreated, control C57BL/6 (B6) and *Il33*$^{-/-}$ mice showed similar plasma P4 concentrations on gestation day (GD) 16.5 and GD17.5 and the same luteolysis-induced decline in plasma P4 evident on GD18.5 (Figure 1A). Plasma P4 concentrations were also similar when the mice were injected daily with 2 mg P4; these concentrations, when measured 24 h post-injection, were ~2–3-fold higher than endogenous P4 concentrations prior to luteolysis (Figure 1A). When given a single injection of 250 μg depot medroxyprogesterone acetate (DMPA; also known as Depo-Provera) on GD12.5, both strains also showed similar plasma MPA concentrations on GD18.5–20.5 (Figure 1B). As expected[12], this depot formulation achieved constant plasma MPA concentrations (Figure 1B), which thus allowed us to create an experimental model that exposed the uterus to an extended period of constant P4 agonist activity, as is normally the case up until the time of luteolysis. Indeed, the injected DMPA was required for the mice to remain pregnant past GD19.5 since they still underwent luteolysis as evidenced by their low plasma P4 concentration on GD18.5 onwards (Figure 1A).

Having thus established that IL-33 deficiency does not affect systemic P4 metabolism, we determined labor onset timing in pregnant B6 and *Il33*$^{-/-}$ mice that were either left untreated, thus allowing parturition to occur secondary to luteolysis, or injected with DMPA on GD12.5, thus obliging it to occur through uterus-intrinsic pathways (Figure 1C). Importantly, since P4 inhibits cervical ripening and dilation in mice[13], we scored labor onset in an inverse fashion, i.e. based upon whether the mice were still pregnant without evidence of dystocia or distress, which would, in addition to delivery itself, indicate the onset of strong uterine contraction (e.g., Figure S1A).

Following mating with B6 males, untreated B6 and *Il33*$^{-/-}$ females both delivered on ~GD19.5 (Figure 1D), in accord with luteolysis occurring 24 h earlier in both strains (Figure 1A). Also as expected, DMPA injection extended gestation length in B6 mice, by ~2–3 days. Accordingly, ~GD22.0 defined the day of labor onset that we consider to be “normal” for mice delivering through uterus-intrinsic pathways. By contrast, labor entry for DMPA-injected *Il33*$^{-/-}$ mice was delayed by yet another ~2 days (Figure 1D). This extended delay was unlikely due to altered P4 sensitivity or metabolism in the uterus, since uterine expression of genes encoding the progesterone receptor (PR; encoded by *Pgr*), 20α-HSD (*Akr1c18*) and the additional P4-metabolizing enzyme steroid 5α-reductase 1 (*Srd5a1*) was unaltered in *Il33*$^{-/-}$ mice (Figure S1B), nor could it be attributed to a difference in fetal or placental growth or the *Il33* heterozygosity of the pups, since fetal and placental weights were similar between the two groups (Figure S1C) and DMPA-injected B6 females mated to *Il33*$^{-/-}$ males entered labor at the same time as DMPA-injected B6 females mated to B6 males (Figure 1D). Litter size was moreover slightly increased in *Il33*$^{-/-}$ mice, a situation that would be expected to predispose towards premature rather than delayed labor onset[2] (Figure S1C). Lastly, the identical parturition timing of untreated B6 and *Il33*$^{-/-}$ mice (Figure 1D) meant that the extended delay of DMPA-injected *Il33*$^{-/-}$ mice could not be explained by intrinsic defects in myometrial contractility. As exemplified by mice with defects in connexin 43 expression by SMCs[14], which prevents these cells from achieving the electrical coupling necessary for synchronous contraction, such defects would be expected to delay luteolysis-driven parturition onset. Together, these results suggest that maternal

IL-33 plays a critical role in labor onset timing in mice when parturition occurs through uterus-intrinsic pathways.

PDGFRα+ interstitial fibroblasts in the myometrium, undecidualized endometrium and mesometrial triangle are the main sources of IL-33 in the pregnant uterus.

In order to identify potential cellular sources of IL-33 within the uterus, we performed a flow cytometric analysis of *Il33*$^{mCherry/+}$ mice bearing a nuclear localized *Il33* reporter construct[15]. For non-pregnant (NP) mice and pregnant mice on GD3.5 (i.e., one day prior to implantation), we analyzed the whole uterus as a unit. For pregnant mice on GD7.5, we dissected the decidua of each implantation site away from its overlying myometrium, and for GD11.5 onwards we additionally separated out the mesometrial triangle, the histologically distinct segment of the myometrium that abuts the decidua basalis (i.e., the portion of the decidua that in turn abuts the placenta; Figure 2A). Importantly, the non-mesometrial triangle portion of the myometrium at these later stages lacks an associated decidua and instead bears an undersurface of undecidualized endometrium replete with luminal epithelial cells (and so hereafter will be referred to as “myo/endo”; see Figure 2C). Accordingly, the decidua basalis constituted the decidual tissue for these later time points. GD20.5 uteri came from mice injected daily with 2 mg P4 for four days starting on GD16.5. As with DMPA injection, this injection regimen, when continued, extended gestation length in B6 mice to ~GD22.5 (data not shown). To assess whether such injections might by themselves affect IL-33mCherry expression, a subset of mice analyzed on GD17.5 were injected daily with P4 for four days starting on GD13.5.

In line with *Il33* being transcriptionally silenced in decidual stromal cells[4], IL-33mCherry expression was not detected in these cells (Figure 2B, S2A and S3A). In contrast, IL-33mCherry was expressed by 10–30% of the stromal cells in the myometrium, myo/endo, and mesometrial triangle (Figure 2B and S3A). Importantly, percentages obtained on GD17.5 were the same whether or not the mice were P4-injected (Figure 2B), demonstrating that *Il33* expression in the prepartum uterus was not itself regulated by P4. Leukocytes were almost completely IL-33mCherry^{-}, and while endothelial and epithelial cells expressed low but appreciable IL-33mCherry in the myo/endo and mesometrial triangle on GD17.5 and GD20.5, they were outnumbered >10-fold by the stromal cells in these tissues (Figure S2B-D).

Importantly, IL-33mCherry expression within the stromal compartment was largely confined to cells expressing PDGFRα, a mesenchymal marker that also identifies IL-33-producing fibroblastic stromal cells in other organs[16] (Figure 2B, S3A). The PDGFRα^{+} cells also expressed Sca-1 (Ly6A) and gp38 (podoplanin), two other stromal markers, but their expression of the contractile markers *Acta2* and *Myh11* was low. These latter markers were instead expressed by the PDGFRα^{-} stromal cells, identifying them as SMCs and/or pericytes (Figure S3B-C). By immunofluorescence, PDGFRα^{+} cells in the late gestation uterus were interspersed between muscle fibers in the myometrium and mesometrial triangle, where they were particularly abundant, and constituted a large fraction of endometrial stromal cells (Figure 2C). SMCs were PDGFRα^{-}, as were decidual stromal cells. Together, these observations indicate that the IL-33-expressing cells of the pregnant

uterus were predominantly PDGFRα$^+$ interstitial fibroblasts, a population that comprises the stroma of the myo/endo and that densely populates the mesometrial triangle.

Il33 deletion in uterine interstitial fibroblasts delays labor onset.

To evaluate the labor induction requirements for IL-33 specifically produced by uterine PDGFRα$^+$ stromal cells, we measured parturition timing in mice bearing floxed *Il33* alleles and either a *Pdgfra-cre* driver to target inactivation to all PDGFRα-expressing cells, or a *Pgr-cre* driver to target inactivation to PR-expressing cells, which reside in reproductive tissues[17] (Figure 3A). In the late gestation uterus, *Pgr-cre*-targeted cells included ~90% of the PDGFRα$^+$ stromal cells in the myo/endo and mesometrial triangle (Figure S4). Importantly, DMPA-treated *Il33*$^{fl/fl}$ mice entered labor at the same time as DMPA-treated B6 mice, confirming that homozygosity for a floxed *Il33* allele by itself had no effect on parturition timing (Figure 3B). By contrast, labor onset in DMPA-treated *Pdgfra-cre Il33*$^{fl/fl}$ mice was delayed 2–3 days compared to DMPA-treated *Pdgfra-cre* mice (Figure 3C), and labor onset in DMPA-treated *Pgr-cre Il33*$^{fl/fl}$ mice was delayed 2–3 days compared to DMPA-treated *Pgr-cre* mice (Figure 3D). Parturition onset in these two latter strains was somewhat earlier than expected considering the labor onset timing of DMPA-treated B6 and *Il33*$^{fl/fl}$ mice, a shift that presumably reflects the fact that the *Pgr-cre* driver is a *Pgr* gene-disrupting allele, and so its presence likely reduces uterine responsiveness to MPA. All strains showed similar delivery times as B6 mice when not treated with DMPA (Figure 3B-D; the lack of an effect of the *Pgr-cre* driver in this case likely reflects the fact that luteolysis is an abrupt event associated with an abrupt decline in plasma P4 concentrations). Together with the IL-33 and PDGFRα expression studies above, these results suggest that PDGFRα$^+$ interstitial fibroblasts of the myo/endo and mesometrial triangle with a history of PR expression are critical local sources of IL-33 when parturition proceeds via uterus-intrinsic pathways.

Prior to labor onset, ILC2s expand in the mesometrial triangle and become highly activated in an IL-33-dependent fashion.

IL-33 binds a dimeric cell surface receptor comprised of the IL-1 receptor accessory protein and an IL-33-specific subunit called ST2 (encoded by *Il1rl1*). Thus, we next performed flow cytometry to identify ST2-expressing cells in the uterus. We expected these cells would potentially mediate the parturition-promoting effects of IL-33, and that their respective activation states, to the extent that they were IL-33-dependent, would indicate presence of intrauterine IL-33 bioactivity. Cells with distinct ST2 staining were ILC2s, fractions of T helper 2 (Th2) and regulatory T (Treg) cells, and eosinophils (Figure S5A-E). Macrophages also stained positive for ST2, albeit dimly (Figure S5C-D). Focusing on the lymphoid compartment, we found that ST2$^+$ ILC2s, Th2 and Treg cells were rare in the NP uterus and the decidua, and that ST2$^+$ Th2 and Treg cell densities were similarly rare in the myometrium, myo/endo, and mesometrial triangle of pregnant mice (Figures 4A and S5F). By contrast, and consistent with prior work[18], ILC2s were present at moderate densities in these latter three tissues, where they constituted ~90% of all ST2$^+$ lymphoid cells. Moreover, ILC2 densities increased ~2-fold in the mesometrial triangle from GD15.5–20.5 (Figure 4A). This increase occurred earlier in B6 mice than in *Il33*$^{-/-}$ mice, revealing not only that

IL-33 promoted uterine ILC2 proliferation and/or accumulation in the prepartum uterus, but also that its impact in the mesometrial triangle started becoming apparent around GD17.5.

Next, we assessed the activation state of uterine ILC2 by measuring production of their signature type 2 cytokines IL-5 and IL-13 (Figure 4B, C). Consistent with prior work[18], all uterine ILC2s in B6 and *Il33*$^{-/-}$ mice expressed at least some amount of IL-5 judged in comparison to isotype-stained controls. In addition, ~30% of ILC2s in the GD7.5 myometrium expressed high amounts of IL-5 as well as IL-13. Such expression was equivalent in B6 and *Il33*$^{-/-}$ mice, indicating that it was not driven by IL-33. IL-5 and IL-13 expression perhaps mildly subsided through mid-gestation but then clearly increased in late gestation in B6 mice starting on ~GD18.5. Particularly high expression was observed in the mesometrial triangle, where ~80% of ILC2s were IL-5^{hi} IL-13^{+} by GD20.5. This late gestational phase of IL-5 and IL-13 expression was not a consequence of the exogenous P4 given to extend gestation length past GD19.5 since uterine ILC2s in B6 mice given the same P4 regimen prior to sacrifice on GD18.5 showed the same percentage of IL-5^{hi} IL-13^{+} cells as their untreated counterparts. On the other hand, IL-5 and IL-13 induction was not observed in *Il33*$^{-/-}$ mice, demonstrating that it required IL-33. These results thus support the idea that IL-33 bioactivity increases within the mesometrial triangle over the few days before labor onset, and suggested a parallel but less intense increase in IL-33 bioactivity in the myo/endo.

We further defined the location of ILC2s in the late gestation uterus by performing thick section immunofluorescence microscopy in conjunction with *Il5-cre*R26RFP mice, which mark as RFP^{+} all cells with a history of IL-5 expression, i.e., ILC2s and rare T cells[16]. In confirmation of our flow cytometric analysis, the marked cells were absent from the decidua on GD17.5 but were present in the myo/endo and mesometrial triangle (Figure 5). In the myo/endo, they were located between muscle fibers and were especially concentrated in the endometrium. In the mesometrial triangle, they showed an association with larger blood vessels and smooth muscle fibers but were otherwise relatively uniformly distributed.

ILC2 depletion or loss of ILC2 responsiveness to IL-33 delays labor onset.

To functionally assess whether IL-33 acts through ILC2s to promote labor onset, we first employed a model of diphtheria toxin- (DT-) inducible ILC2 depletion (*Il5-cre* iDTR mice) in which the constitutively active *Rosa26* locus expresses a Cre-inducible DT receptor (iDTR), and one *Il5* locus bears a gene targeted Cre construct to direct iDTR expression to cells with a history of IL-5 expression (i.e., ILC2s and rare T cells, as above). Accordingly, DT injection every other day from GD12.5 achieved a ~50% decrease in ILC2 density in the myo/endo and mesometrial triangle by GD18.5 compared to control, DT-treated *Il5-cre* mice (Figure 6A). When given DMPA, these DT-treated mice showed a ~1–2 day extended delay in labor onset compared to control DMPA- DT-treated *Il5-cre* mice, which themselves showed no difference in labor onset timing compared to DMPA-treated *Il5-cre* mice (Figure 6B). We also evaluated parturition timing in *Il5-cre Il1rl1*$^{fl/fl}$ mice in which *Il1rl1* deletion is similarly targeted to ILC2s and rare T cells. These mice demonstrated a loss of surface ST2 on ~75% of uterine ILC2s (Figure 6C), and, with DMPA-treatment, a ~2-day extended delay in labor onset compared to control DMPA-treated *Il5-cre* and DMPA-treated *Il1rl1*$^{fl/fl}$ mice

(Figure 6D). By contrast, DMPA-treated *Rag2*$^{-/-}$ mice deficient in T and B cells but not ILC2s delivered at the same time as DMPA-treated B6 mice (Figure 6E). All these strains delivered at the same time as B6 mice when not given DMPA (Figure 6B, 6D and 6E). Together, these data indicated that IL-33 promotes labor onset through effects on ILC2s, potentially including those residing in the uterus.

Decidual *Ptgs2* induction is downstream of IL-33 in the prepartum uterus, but is non-essential for on time labor onset.

We next sought additional insight into IL-33-induced parturition mechanisms by performing RNA-sequencing (RNA-Seq) on dissected uterine tissue layers of pregnant B6 and *Il33*$^{-/-}$ mice. The tissues were collected on GD18.5 and the mice were not treated with DMPA nor P4. Notably, the gene expression differences across the two genotypes were relatively minor, with almost no difference reaching an *FDR* of less that 0.05 (Figure S6A, Supplemental Table 1, and GSE181904). This lack of a difference was consistent with the lack of a parturition delay in *Il33*$^{-/-}$ mice when luteolysis was available to induce labor onset (Figure 1D), and reinforced the notion that the parturition delay in DMPA-treated *Il33*$^{-/-}$ mice was not due to a cell-intrinsic defect in myometrial SMC maturation or function. The expression of genes encoding ILC2-derived factors such as IL-5 and IL-13 were not detectable in mice of either genotype, likely reflecting the relative scarcity of uterine ILC2s.

Despite so few expression differences, *Ptgs2*, encoding the prostaglandin synthesis enzyme COX-2, emerged as the most down-regulated protein-coding gene in the *Il33*$^{-/-}$ decidua on GD18.5 (~2.5-fold, p_{raw}=0.007; Figure S6A). This observation was notable since COX-2 induction is the signature hallmark of "decidual activation," a poorly understood process that has nonetheless been considered a key event in human parturition given the contractile effects of the prostaglandin species consequently produced[7]. Indeed, *Ptgs2* mRNA and COX-2 protein expression were also lower on GD20.5 in the *Il33*$^{-/-}$ decidua (Figure S6B-C), as were PGE2 concentrations, a finding attributable to reduced production rather than increased metabolism since decidual concentrations of PGE metabolites were reduced in parallel on GD20.5 and were almost undetectable in the *Il33*$^{-/-}$ decidua (Figure S6D). In contrast to the decidua, *Ptgs2* expression was unaltered in the myo/endo and mesometrial triangle, where absolute expression was much less to begin with (Figure S6B). In addition, the expression of *Ptgs1*, encoding the second prostaglandin synthesis enzyme COX-1, as well as the concentrations of $PGF_{2\alpha}$ and PGD2, prostaglandin species produced at high amounts in the prepartum mouse uterus in a COX-1-dependent fashion[19-21], were unaltered in all tissue layers (Figure S6D).

Notwithstanding these indications that IL-33 might promote parturition onset by inducing decidual COX-2 expression, the injection of DMPA-treated B6 mice with SC-236, a long-acting and selective COX-2 inhibitor, did not further extend gestation length (Figure S6E). As expected[22], the same dosing nonetheless inhibited inflammation-induced PTL (data not shown). Thus, decidual COX-2 induction was not a key component of the IL-33-regulated parturition cascade. These observations are in line with the thought that COX-2-derived prostaglandins foster the progression of non-inflammation-associated labor rather than trigger its onset[23]. Moreover, they raise the possibly that decidual activation, rather than

being a determinant of labor onset timing in humans as has been suggested[7], is instead a byproduct of labor-inducing events taking place in the myometrium.

Eosinophil turnover increases in the prepartum uterus and IL-5 is required for on time labor onset via uterus-intrinsic parturition pathways.

Given their function as IL-33- and IL-5-regulated effectors of type 2 immunity, we next evaluated the possibility that eosinophils instead served as effectors of the labor cascade. On GD16.5, uterine eosinophils were rare and their densities were respectively similar in B6 and *Il33*$^{-/-}$ mice across all three tissue layers, with P4 treatment causing mild, genotype-independent and largely statistically insignificant density reductions (Figure 7A). After this point, however, eosinophil densities diverged between the two genotypes, with *Il33*$^{-/-}$ mice showing marked reductions on GD18.5 (in P4-untreated mice) and GD20.5 (in P4-treated mice) in all tissue layers (Figure 7A). Indeed, eosinophils were barely detectable in the GD18.5 and GD20.5 myo/endo and mesometrial triangle of *Il33*$^{-/-}$ mice. A parallel decline was also apparent in B6 mice, but it was more modest. Uterine eosinophil tissue densities were consequently much lower in *Il33*$^{-/-}$ mice than in B6 mice on GD18.5 and GD20.5 (Figure 7A). Importantly, blood eosinophil frequencies were also greatly reduced in *Il33*$^{-/-}$ mice (Figure 7B, left). This observation is consistent with prior work establishing that IL-33 is required for optimal eosinophilopoiesis[24] and suggested that the pronounced loss of eosinophils from the prepartum uteri of *Il33*$^{-/-}$ mice was at least partly due to their paucity of blood eosinophils. Consistent with this possibility, *Pgr-cre Il33*$^{f/f}$ mice with reproductive tissue-targeted *Il33* deletion showed similar uterine eosinophil densities on GD20.5 compared to both *Pgr-cre* and B6 controls, and a less severe and statistically insignificant reduction in blood eosinophil frequencies compared to B6 mice (Figure 7B, 7C; of note, within the interpretive limits imposed by the wide variance of these data, blood eosinophil frequencies in *Pgr-cre Il33*$^{f/f}$ and *Pgr-cre* mice were similar to each other yet somewhat reduced compared to B6 mice suggesting that the loss of one *Pgr* allele affects eosinophilopoiesis). Our findings with respect to gestation day- and genotype-dependent differences in uterine eosinophil tissue densities were corroborated when we calculated eosinophils as percentages of the total leukocytes that respectively reside within each uterine tissue layer (Figure S7A, 7B). Together, these observations thus suggest that uterine eosinophil turnover increases over the days leading up to labor onset, potentially through uterine IL-33-independent pathways, with increased recruitment from the blood necessary to offset increased intrauterine eosinophil death. Such death could be the result of the eosinophils performing death-inducing effector functions such as cytolysis[25].

To gain further support for the idea that eosinophil turnover increases in the prepartum uterus, we took advantage of the prior observation that eosinophils with longer tissue-residence times upregulate expression of the integrin subunit CD11c in certain contexts[26]. Accordingly, we assessed CD11c expression by uterine eosinophils in P4-injected B6 mice while also employing the intravenous injection of PerCP-Cy5.5-conjugated anti-CD45 antibodies to discriminate extravascular (PerCP-Cy5.5^{lo}) from intravascular (PerCP-Cy5.5^{hi}) cells[27] (Figure 7D, 7E). As expected, uterine eosinophils in the intravascular compartment did not express CD11c. By contrast, ~25–35% of the extravascular eosinophils in the myo/endo and mesometrial triangle were CD11c^{+} on GD16.5, suggesting that at least these

cells were not recent recruits from the blood. On GD20.5, however, $CD11c^+$ percentages had substantially declined. These observations were consistent with the idea that eosinophil turnover increases in the uterus prior to labor onset since they implied that the cells with longer tissue residence had died and that the dynamics of the remaining cells were not at steady-state.

Of note, exogenous P4 treatment increased the percentage of $CD11c^+$ cells in the GD16.5 myo/endo and mesometrial triangle of both B6 and *Il33*$^{-/-}$ mice (Figure S7C). Together with its aforementioned ability to mildly reduce uterine eosinophil tissue densities (Figure 7A), exogenous P4 thus appeared to have a suppressive effect on uterine eosinophil turnover in the prepartum uterus. This possibility is consistent with the known effects of ovarian hormones on uterine eosinophil dynamics[28,29]. Locally-produced factors also appeared to control eosinophil phenotypes in the prepartum uterus, as CD11c expression by decidual eosinophils was low on GD16.5 in mice injected with P4 (Figure 7D, 7E, and S7C).

Lastly, we assessed parturition timing in *Il5*$^{-/-}$ mice to determine whether eosinophils functionally contributed to uterus-intrinsic parturition pathways. IL-5 is an activator of mature eosinophils as well as a critical eosinophil development and survival factor, as demonstrated by the profound reductions in eosinophil numbers in the blood and tissues of *Il5*$^{-/-}$ mice[25,30,31]. Such reductions were also apparent in the late gestation uterus of *Il5*$^{-/-}$ mice (Figure S7D). As expected from prior work[32], *Il5*$^{-/-}$ mice delivered on time when not DMPA-treated. In contrast, DMPA-injected *Il5*$^{-/-}$ mice showed an extended delay in parturition onset compared to DMPA-injected B6 controls (Figure 7F). Since an extended parturition delay was not apparent in DMPA-injected *Rag2*$^{-/-}$ mice deficient in B cells (Figure 6E), the only other cell type thought to be a direct IL-5 target in mice[30,33], these observations strongly implicated a role for eosinophils in uterus-intrinsic parturition pathways. Of note, the injection of DMPA-treated B6 mice with antibodies towards CCR3, a chemokine receptor expressed by eosinophils, did not appreciably extend gestation length compared to isotype-injected controls (Figure S7E). As expected from the ability of these antibodies to deplete eosinophils[34], this injection substantially depleted eosinophils from the blood as well as from the GD20.5 decidua and mesometrial triangle (Figure S7D, S7F). However, eosinophil depletion was less robust in the myo/endo, and the depletion seen in the decidua did not reach that achieved by IL-5 deficiency (Figure S7F). Together with the observation of delayed onset in *Il5*$^{-/-}$ mice, these data suggest that eosinophils in the myo/endo and possibly the decidua are sufficient to trigger on time labor onset. They are also consistent with the idea that IL-5 produced within the uterus helps to locally activate eosinophils to promote labor onset. It is also possible that IL-5 promotes labor onset by acting on a previously unrecognized non-eosinophil, non-B cell target cell within the uterus.

DISCUSSION

Mechanisms of parturition induction, a question with major implications for maternal-fetal health, remain largely undefined. In this study, we dissect these mechanisms in mice under experimental conditions that oblige labor onset to rely upon uterus intrinsic pathways, as they normally do in humans. Under these conditions, we implicate several components of innate type 2 immunity as key contributors of the parturition cascade.

These findings contrast with prior ones that ruled out roles for components of type 2 immunity when parturition is driven by luteolysis (e.g., in mast cell- and eosinophil-deficient mice[32,35]), thus emphasizing the different physiologies at play and revealing that exogenous progestin administration can be used to uncover previously unrecognized components of the parturition cascade.

Importantly, some of our experiments employed mice with systemic defects in type 2 immunity. In these cases, we cannot directly establish the extent to which parturition delay phenotypes are due to altered immune activity within the uterus itself. For example, reduced eosinophilopoiesis likely contributes to the extended parturition delay of DMPA-treated *Il33*$^{-/-}$ mice given that eosinophils are themselves required for on time parturition onset and their low frequency in the blood likely contributes to their low tissue densities in the prepartum *Il33*$^{-/-}$ uterus. Similarly, reduced eosinophilopoiesis likely contributes to the parturition delays of DMPA-treated *Il5-cre* iDTR mice and *Il5-cre Il1rl1*$^{fl/fl}$ mice, given that *Rag2*$^{-/-}$ *Il2rg*$^{-/-}$ mice lacking ILC2s and *Il1rl1*$^{-/-}$ mice with global ST2 deficiency also bear reduced numbers of blood eosinophils[24,26]. However, our data also reveal increased activity of type 2 immunity in the prepartum uterus and a local requirement for this activity in stimulating labor onset. Specifically, in the days leading up to labor onset we observed increased uterine eosinophil turnover and IL-33-dependent expansion and activation of uterine ILC2s, as well as an extended parturition delay in DMPA-treated *Pgr-cre Il33*$^{f/f}$ mice. These latter mice target *Il33* deletion to cells of reproductive tissues, including the interstitial fibroblasts of the uterus that express high amounts of IL-33. Moreover, they did not show reductions in uterine eosinophil tissue densities, indicating that their parturition delay is independent of processes that might reduce eosinophil numbers in the uterus.

Considering how type 2 immune circuitry within peripheral tissues is currently conceptualized, these observations suggest a two-pronged general model for how type 2 immunity promotes labor onset in mice. In the first prong, IL-33 activity is generated in the prepartum uterus and acts locally on ILC2s, eosinophils, and other IL-33 responsive cells. These latter cells likely include uterine macrophages, given that they express low amounts of ST2, as well as mast cells given that mast cells are present in the mouse uterus and classically express ST2[9,35], even though we could not detect them by flow cytometry. In response, these cell types produce factors that in turn directly or indirectly promote uterine SMC contraction, perhaps in ways that are akin to those that promote SMC contraction in the lung and gut during classical type 2-associated immune responses (asthma, helminth clearance, etc.). In the second prong, prepartum activation of an as yet unidentified but IL-33-independent pathway promotes uterine eosinophil turnover and perhaps also eosinophil effector function. This pathway appears to be active within all uterine tissue layers and might also contribute to the component of ILC2 expansion in the prepartum mesometrial triangle that is IL-33-independent. It also appears to be suppressed by P4 given that the uterine eosinophils of mice supplemented with exogenous P4 prior to sacrifice on GD16.5 show increased positivity for CD11c and slight reductions in uterine eosinophil tissue densities.

Although many details of this model remain to be clarified, it is worth specifically discussing how IL-33 bioactivity might be generated in the late gestation uterus, since

elucidation of this question could help identify more upstream components of the labor cascade. One possibility is that it is generated by the low-grade inflammation characteristic of the late gestation uterus[6,7]. This idea is in line with the classical view of IL-33 being a nucleus-sequestered alarmin released in response to noxious stimuli, as well as with the ability of inflammation-associated proteases to process IL-33 into more active forms[9,36]. Such inflammation might be related to the second prong of type 2 immune activation mentioned above. Uterine stretch might also generate IL-33 bioactivity given that IL-33 can be released from living cells in response to mechanical tension[37]. Lastly, given that ILC2s are regulated by multiple factors, it is possible that their activation in late gestation does not reflect greater IL-33 bioactivity per se, but rather synergy between constant ST2 signaling and increased signaling via other inputs.

Of note, PGD2, another type 2 immune regulator with activating and chemotactic effects on ILC2s and eosinophils[38], is abundantly produced in the prepartum uterus in a COX-1-dependent fashion (refs. [19,20]). Due to its pro-contractile effects on myometrial tissue strips assayed *in vitro*, this prostaglandin species has been suggested to contribute to labor induction by directly promoting myometrial SMC contractility[19,39]. However, our results raise the possibility that it may also promote labor onset in part by stimulating type 2 immunity, potentially as a component of the second prong described above given that its production is not dependent upon IL-33. Additional work will be required to evaluate this possibility. Additional work will also be required to evaluate the roles of factors produced by ILC2s, which in the context of the prepartum uterus may be complex. For example, uterine ILC2-derived IL-5 might promote both the survival and death of uterine eosinophils through inhibitory and stimulatory effects on eosinophil apoptosis and effector function, respectively[25,31].

Further evaluation of the role of type 2 immunity in mouse parturition will also need to consider the seemingly specialized function of the mesometrial triangle, with its massive population of IL-33-expressing interstitial fibroblasts and its accumulation of ILC2s that become activated in late gestation and localize to larger blood vessels and dispersed muscle fibers. This structure also houses large numbers of NK cells and dendritic cells[27,40], and appears to originate the electrical activity that drives uterine contractions[41]. We therefore speculate that it serves as a hub that integrates information from multiple sources to ensure that labor commences only when all tissue compartments are sufficiently mature. Indeed, the potential importance of the mesometrial triangle is also suggested by the upstream role of IL-33 in promoting decidual activation, even though such activation appears to be non-essential for on time labor onset.

Of note, potential roles for IL-33 in mouse pregnancy prior to labor onset were the subject of a recent paper by Valero-Pacheco et al.[42]. This paper identified the interstitial fibroblasts of the myo/endo as the major producers of IL-33 of the pregnant uterus, in accord with the data presented here. However, we could not confirm certain other aspects of the work, including its suggestion that decidual stromal and endothelial cells are major IL-33 producers, or that maternal IL-33 deficiency mildly reduces fetal weights and litter sizes in late gestation. The study also reported that IL-33 deficiency alters the development and vascularization of GD7.5–9.5 implantation sites. While provocative with respect to mechanisms of early

pregnancy success or failure, such alterations are unlikely the cause of the parturition delay seen in *Il33*$^{-/-}$ mice, since this delay was also apparent when we ablated ILC2s starting on GD12.5. Moreover, since our RNA-Seq analysis performed on GD18.5 revealed only minimal gene expression differences between the respective uterine tissue layers of B6 and *Il33*$^{-/-}$ mice, the alterations observed in early gestation by Valero-Pacheco et al. did not appear to have substantial downstream consequences for late gestation.

Although our use of progestin supplementation creates an endocrine state in mice that models the conditions under which parturition occurs in humans, further work will be needed to determine the extent to which the pathways we thus uncovered are relevant to humans. Notably, increased circulating concentrations of soluble ST2, a secreted, alternative splice form of ST2 that acts as an IL-33 decoy receptor, has recently been reported as being predictive of impending labor onset in pregnant women[43]. These observations were interpreted as reflecting a labor-inhibiting role for IL-33, in line with suggestions stemming from work on PTL pathways in mice[44]. However, this latter study did not directly assess labor onset timing in *Il33*$^{-/-}$ mice, and the increase in circulating soluble ST2 in humans might instead reflect a counter-regulatory response induced by the low-grade inflammation characteristic of the prepartum uterus[6,7] given that inflammation is frequently associated with increased soluble ST2 production[45]. Indeed, our data showing that type 2 immunity is required for on time labor onset in mice is consistent with several lines of evidence suggesting that type 2 immunity promotes parturition in humans. Most recently, ILC2s have been detected in the human decidua basalis at term and have been shown to be the most abundant ILC in the human decidua parietalis, a tissue layer that is anatomically analogous to the undecidualized endometrium on the undersurface of the mouse myometrium where we find ILC2s to be abundant. In both locations, the cells show increased densities in cases of PTL[46,47]. Older data has moreover found associations with PTL and the presence of eosinophils in the amniotic fluid, and case reports exist of type I allergic reactions triggering PTL[48,49]. Type I allergic reactions can also trigger PTL in guinea pigs, which, like humans, enter labor without a drop in plasma P4 concentrations[50]. Whether or not ILC2s are present in the human myometrium has not yet been described, and unfortunately their scarcity may preclude their detection by single cell RNA sequencing. Together, however, these results indicate the ability of type 2 immune pathways to foster pathological labor onset in humans, raising the possibility that components of these pathways also contribute to normal parturition.

LIMITATIONS OF THE STUDY

This study presents evidence that innate type 2 immunity plays an important role in the control of parturition onset in mice when their endocrine state is manipulated experimentally to mimic the context of human parturition. One limitation of our study is our use of genetic models with systemic immunological effects. This limits our ability to interpret certain cases of delayed parturition as being due to altered activity of cells residing within pregnant uterus itself. Although mitigated by the delayed parturition phenotype of *Pgr-cre Il33*$^{f/f}$ mice with reproductive tissue-targeted IL-33 deficiency, this limitation applies to experiments using *Il33*$^{-/-}$, *Il5-cre* iDTR and *Il5-cre Il1rl1*$^{fl/fl}$ mice. Given the systemic loss of eosinophils seen in *Il5*$^{-/-}$ mice, we are similarly unable to determine the extent to which ILC2-derived IL-5

promotes parturition onset by locally activating uterine eosinophils. We moreover cannot rule out the possibility that IL-5 promotes parturition onset through direct effects on a non-eosinophil, non-B cell target cell expressing the IL-5 receptor. Our study does not identify upstream triggers of innate type 2 immune activity within the late gestation uterus, nor how such activity leads to increased myometrial contractility. Lastly, we present progestin supplementation in mice as an experimentally tractable model for dissecting parturition mechanisms potentially relevant to human parturition. Whether activation of innate type 2 immunity, which we thus uncover as an important mechanism in this context, plays a role in human parturition will need its own direct experimental validation. Additional experiments are also needed to assess the role of innate type 2 immunity in inflammation-induced preterm birth in both mice and humans.

STAR METHODS

RESOURCE AVAILABILITY

Lead contact—Further information and requests for resources and reagents should be directed to and will be fulfilled by the lead contact, Adrian Erlebacher (adrian.erlebacher@ucsf.edu).

Materials availability—This study did not generate new unique reagents.

Data and code availability—The RNA-seq data generated in this study have been deposited in the Gene Expression Omnibus (GEO) database and are publicly available as of the date of publication. The accession number is listed in the key resources table. This paper does not report original code. Any additional information required to reanalyze the data reported in this paper is available from the lead contact upon request.

EXPERIMENTAL MODEL AND SUBJECT DETAILS

Mice—C57BL/6J (B6), *Pdgfra-cre* (C57BL/6-Tg(Pdgfra-cre)1Clc/J), iDTR (C57BL/6-*Gt(ROSA)26Sor*$^{tm1(HBEGF)Awai}$/J), *Rag2*$^{-/-}$ (B6.Cg-*Rag2*$^{tm1.1Cgn}$/J), and mTmG (B6.129(Cg)-*Gt(ROSA)26Sor*$^{tm4(ACTB-tdTomato,-EGFP)Luo}$/J) mice were purchased from The Jackson Laboratory and were all on a B6 background. *Il33*$^{-/-}$ mice (*Il33*$^{Gt/Gt}$; ref. [51]) were the gift of Jean-Philippe Girard, B6(C)-*Il5*$^{tm1.1(icre)Lky}$/J mice (*Il5-cre*; ref. [52]) were the gift of Richard Locksley, *Il33*$^{fl/fl}$ and *Il1rl1*$^{fl/fl}$ mice[53] were the gifts of Richard Lee, B6.*Il33*$^{mCherry/mCherry}$ (IL-33mCherry) mice[15] were the gift of Marco Colonna, and *Pgr-cre* mice[17] were the gift of Francesco DeMayo and John Lydon. If not already on a B6 background, all mice were backcrossed with B6 mice to reach at least N10. Mice were heterozygous for the *Il5-cre* allele, which causes *Il5* gene disruption, when the allele was used to target gene deletion to IL-5-expressing cell types. It was intercrossed to homozygosity to generate IL-5-deficient (*Il5*$^{-/-}$) mice. *Il5-cre* B6.Cg-*Gt(ROSA)26Sor*$^{tm14(CAG-tdTomato)Hze}$/J (*Il5-cre*R26RFP) mice have been described previously[16]. *Il33*$^{fl/fl}$ mice were intercrossed with *Pgr-cre* mice to generate *Pgr-cre Il33*$^{fl/fl}$ mice or with *Pdgfra-cre* mice to generate *Pdgfra-cre Il33*$^{fl/fl}$ mice. *Il5-cre* mice were intercrossed with iDTR mice to generate *Il5-cre* iDTR mice or with *Il1rl1*$^{fl/f}$ mice to generate *Il5-cre Il1rl1*$^{fl/f}$ mice. *Pgr-cre* mice were intercrossed with mTmG mice, modified

to include sequences encoding ovalbumin-derived peptides as described in the Figure S4 legend, to generate the mice for the lineage tracing experiment. The mice were maintained in specific pathogen-free animal barrier facility at UCSF. In order to maintain a consistent microbiota, all females used for experiments were born in the Erlebacher lab holding room except for the mice used for Figure 5, which were born in the Molofsky lab holding room, and the mice used for the anti-CCR3-mediated eosinophil depletion experiment, which were purchased from The Jackson Laboratory. All experiments were performed using female mice because only females become pregnant. Virgin females, 6–10 weeks old, were used for all experiments and were mated to B6 males unless otherwise indicated. All experiments were approved by the UCSF IACUC (Protocols #AN178689 and #AN193713).

METHODS DETAILS

Pregnancy experiments—Vaginal plugs were checked in the mornings, and noon of that day was counted as GD0.5. To determine labor onset timing, pregnant mice were checked twice daily (9 am and 6 pm) for evidence of delivery, uterine bleeding, or maternal distress. If apparent at 9 am, labor onset timing was scored as GDX.5, with X being the number of days after mating (i.e., GD0.5). If apparent at 6 pm, it was scored as GD(X+1).0 (i.e. midnight of the next gestation day). For parturition timing experiments, pregnant mice were injected subcutaneously with a single dose of 250 μg depot medroxyprogesterone acetate (DMPA; Depo-Provera, Pfizer) in 100 μl PBS on GD12.5. This dose was chosen because it was the minimum needed to consistently extend gestation length in B6 mice past 24 h. To analyze mice on GD20.5, gestation was extended by giving subcutaneous daily injections of 2 mg P4 (Sigma-Aldrich) dissolved in 0.1 ml sesame seed oil (Sigma-Aldrich) starting on GD16.5. To control for the effect of these injections, some mice were analyzed on GD16.5 or GD17.5 after they received subcutaneous daily injections of 2 mg P4 starting on GD12.5 or GD13.5, respectively. Non-pregnant mice were injected with P4 for the 3 days prior to sacrifice in order to mimic the endocrine state of pregnancy. *Il5-cre* iDTR and *Il5-cre* mice received intraperitoneal injections of 300 ng diphtheria toxin (Calbiochem) in 200 μl PBS every other day until the mice delivered or when they reached the end point of the experiment. The COX-2 specific inhibitor SC-236 (Axon Medchem) was injected intraperitoneally at 6 mg/kg in 200 μl 50:50 PBS:DMSO. Anti-CCR3 antibodies and isotype control antibodies (clones 6S2–19-4 and LTF-2, respectively; Bio-X-Cell), were intravenously injected on GD16.5 at a dose of 500 μg in 100 μl PBS.

Tissue digestion and flow cytometry—Non-pregnant and GD3.5 uteri were digested as whole tissues. For pregnant mice on GD7.5, the decidua was separated from the overlying myometrium. From GD11.5 to GD20.5, the myometrium and mesometrial triangle were further separated. As previously described[54], tissues and tissue layers were enzymatically disaggregated via incubation in Liberase™ TL Research Grade (50 μg/ml; Roche), DNAse I (30 μg/ml; Roche) and trypsin (0.05%; ThermoFisher Scientific) in HBSS buffer for 45 min at 37° C, with trituration every 10 minutes. EDTA was then added to a 5 mM final concentration and the samples were incubated 15 minutes more at 37° C. The cell suspensions were then filtered through 40 μm nylon mesh, and washed in PBS. For surface staining, the cells were first incubated with rat anti–mouse CD16/CD32 (BioXCell, clone 2.4G2; 5 μg/ml for 1×10^6 cells) to block nonspecific antibody

binding. Antibodies, purchased from BD Biosciences, BioLegend, Invitrogen, or MD Bioproducts were: FITC-conjugated anti-CD102 (clone 3C4), Bv-711 or PE-Cy7-conjugated anti-CD326 (EpCAM clone G8.8), PE or APC-conjugated anti-CD140a (clone APA5), APC-Cy7-conjugated anti-gp38/podoplanin (clone 8.1.1), BV711-conjugated anti-Ly-6A/E (Sca-1 clone D7), PE-conjugated anti-CD54 (clone YN1/1.7.4), PerCP-Cy5.5- or BUV395-conjugated anti-CD45 (clone 30-F11), BV711-conjugated anti-CD4 (clone RMA4–5), BV605-conjugated anti-CD11b (clone M1/70), APC-Cy7-conjugated anti-NK1.1 (clone PK136), PE/Dazzle594-conjugated anti-CD19 (clone 6D5), PE-conjugated anti-T1/ST2 (clone DJ8), BV421-conjugated anti-CD90.2 (Thy1.2 clone 53–2.1), AF700-conjugated anti-CD3 (clone 17A2), APC-conjugated anti-Ly-6G (clone 1A8), FITC-conjugated anti-F4/80 (clone BM8), BV421-conjugated anti-Siglec-F (clone E50–2440), BV650-conjugated anti-CD11c (clone N418). Intracellular staining was performed after surface staining using PE-Cy7-conjugated anti-FOXP3 (clone FJK-16s), eFluor-660-conjugated anti GATA3 (clone TWAJ), PE-Cy7-conjugated anti-IL-13 (clone eBio13A), and anti-IL-5 (clone TRFK5) followed by FITC-conjugated anti-rat IgG1 (clone MRG1–58). For the detection of IL-5 and IL-13 expression, 1 ml cell suspensions in RPMI/10% FBS were incubated with 50 ng/ml phorbol 12-myristate 13-acetate (PMA; Adipogen) and 500 ng/ml ionomycin (Adipogen) for a total of 4 h. Brefeldin A (1 μl of GolgiPlug™, BD Biosciences) and 2 μM monensin (Abcam) secretion inhibitors were added to the culture after 1 h. Live/dead discrimination employed Fixable Viability Dye eFluor 506 (Invitrogen).

To visualize IL-33mCherry expression among the major uterine cell lineages, leukocytes were identified as $CD45^+$ cells, stromal cells as $CD45^-$ $EpCAM^-$ $CD102^-$ cells, epithelial cells as $CD45^-$ $CD102^-$ $EpCAM^+$ cells, and endothelial cells as $CD45^-$ $EpCAM^-$ $CD102^+$ cells (see Figure S2A). The stromal cells were further subdivided based upon their staining with antibodies to PDGFRα, Sca1 and gp38. The same scheme was used for the lineage tracing experiments (Figure S4), except that CD54 instead of CD102 was used to identify endothelial cells (see Figure S4A). For leukocyte analyses, the mice were injected intravenously with PerCP-Cy5.5-conjugated anti-CD45 antibodies 5 minutes prior to sacrifice in order to discriminate intravascular from extravascular cells[27]. ILC2s were identified as $CD45^+$ lin^- ($CD11b^-$ $CD3\varepsilon^-$ $CD4^-$ $CD19^-$ $NK1.1^-$) Thy1.2 $(CD90.2)^+$ $GATA3^+$ IL1RL1 $(ST2)^+$ cells (or just as $CD45^+$ lin^- $Thy1.2^+$ $GATA3^+$ cells in the case of *Il5-cre Il1rl1*$^{f/f}$ mice). Treg cells were identified as $CD45^+$ $CD11b^-$ $CD3\varepsilon^+$ $CD4^+$ $FOXP3^+$ cells; Th2 cells were identified as $CD45^+$ $CD11b^-$, $CD3\varepsilon^+$, $CD4^+$, $FOXP3^-$, $GATA3^+$ cells. Eosinophils were identified as $CD45^+$ $CD11b^+$ Ly-$6G^-$ F4/80^{int} Siglec-F^+ cells. Intravascular cells were identified as PerCP-$Cy5.5^{hi}$ and extravascular cells as PerCP-$Cy5.5^{lo}$. Samples were run on a five-laser LSRFortessa™ X-20 (BD Biosciences) and data were analyzed using FlowJo software (Tree Star, USA) and compiled using Prism (GraphPad). Cell counts were performed using flow cytometry counting beads (CountBright Absolute™; Life Technologies) per the manufacturer's instructions. For Figure S3B, stromal cells from the GD18.5 myo/endo of B6 mice were gated as live ($DAPI^-$) $CD45^-$ $CD102^-$ $EpCAM^-$ cells and sorted based upon their relative expression of PDGFRα using a MoFlo XDP (Beckman Coulter).

Thin section immunofluorescence—Uterine tissues were fixed overnight at 4°C in 4% paraformaldehyde/PBS and embedded in paraffin. Sections were cut at 5 μm, baked 30 min at 65˚C, then deparaffinized in xylene and ethanol using standard methods. The slides were incubated in methanol for 5 min, air-dried for 30 min, and then incubated with 3% H_2O_2/0.1% sodium azide in PBS for 30 min. The sections were then subjected to antigen retrieval in 10 mM citrate pH 6.0 using a Biocare Decloaking chamber™ NxGen (110°C for 30 sec, allowed to cool down for 10 min in the chamber, then 5 min at room temperature). The sections were then blocked in 1% BSA/3% donkey serum/0.4% Triton X-100 for 1 h at room temperature, followed by application of primary antibodies, diluted in 1% BSA, 0.4% Triton X-100, and incubation at 4°C overnight. Antibody sources, dilutions and antigen retrieval methods were as follows: AF488-conjugated mouse anti-smooth muscle actin (α-SMA, clone 1A4, eBioscience; 1:100), AF647-conjugated mouse anti-α-SMA (clone 1A4, Novus Biological; 1:1000), rabbit anti-PDGFRα (clone EPR22059–270, Abcam; 1:1000), and rabbit anti-COX-2 (clone D5H5, Cell Signaling Technology; 1:1000).

The slides were washed three times in PBS between all subsequent steps. The PDGFRα and COX-2 immunostaining employed biotin tyramide amplification, and so the sections were next incubated for 30 min at room temperature with horseradish peroxidase- (HRP-) conjugated donkey anti-rabbit IgG-secondary antibodies (Jackson ImmunoResearch) diluted 1:200 in TNB blocking buffer (PerkinElmer). They were then incubated in 1.8 μg/mL biotin-tyramide/0.0015% H_2O_2/PBS for 5 min at room temperature, then in 5 μg/ml streptavidin-Alexa Fluor 594 for 30 min at room temperature, and then mounted using DAPI mounting media (Electron Microscopy Sciences). All immunofluorescence images were captured using an Axio Imager M2 microscope running on Zen software (Zeiss). Panoramic views were generated by tiling images taken with the 10X objective. Adobe Photoshop was sometimes used to increase image brightness using the brightness/contrast function; in these cases, the alteration was applied over the entire image and was equally applied to all images within an experiment.

Thick section immunofluorescence—Implantation sites of GD17.5 *Il5-cre*R26RFP mice were harvested and fixed in fresh 4% paraformaldehyde overnight at 4°C, after embryos were removed. After washing with 1X PBS, 300 μm sections were prepared using a vibrating microtome (Precisionary Compresstome VF-310–0Z). Tissue sections were then dehydrated through a methanol/H_2O series (20%, 40%, 60%, 80%, 100%; 10 min each), bleached in chilled fresh 5% H_2O_2/methanol for 2 h at 4°C, then rehydrated with the above methanol/H_2O series (10 min each). The sections were then washed and incubated in permeabilization buffer (PBS/0.2% Triton X-100/0.3 M glycine) for 24 h at room temperature, blocked in PBS/0.2% Triton X-100/5% donkey serum overnight at 4°C, washed again in PBS/0.2% Tween-20, then incubated with primary antibodies diluted in PBS/0.2% Tween-20/3% donkey serum overnight at room temperature. The sections were then washed 3–4 times in PBS/0.2% Tween-20 for 30 min each, incubated with secondary antibodies diluted in PBS/0.2% Tween-20/3% donkey serum at room temperature for 6–8 h, washed in PBS/0.2% Tween-20 for 1 day, dehydrated in an ascending ethanol series (20%, 30%, 50%, 70%, 95%, 100%; 10 min each), then cleared in methyl salicylate.

To visualize RFP^+ ($tdTomato^+$) cells, sections were stained with anti-DsRed antibodies (Living Colors anti-DsRed rabbit polyclonal, Takara Bio; 1:500), concurrently with rat anti-CD31 antibodies (MEC13.3, Biolegend; 1:100) to visualize endothelial cells, and AF488-conjugated anti-α-SMA antibodies (clone 1A4, eBioscience; 1:200) to visualize SMCs. AF555-conjugated donkey anti-rabbit IgG (ThermoFisher Scientific) and AF647-conjugated donkey anti-rat IgG (Abcam) were used as secondary antibodies at 1:400 dilution.

Stained slides were scanned using a Nikon A1R laser scanning confocal microscope equipped with 405, 488, 561, and 650 nm lasers and a 16X/0.8 Plan Apo long working distance water immersion objective. Z steps were acquired every 6 μm, and Z-stacks were rendered in 3D dimensions and quantitatively analyzed using Bitplane Imaris v9.7 software package (Andor Technology PLC). RFP^+ cells were identified and surfaced using the Imaris spots function based on the anti-RFP fluorescence signal together with the Ortho slicer function to filter for size and morphology.

RNA-Seq and qRT-PCR—Whole tissue layers were homogenized in TRIzol (Thermo Fisher Scientific), and RNA was isolated according to the manufacturer's instructions. For RNA-Seq, the samples were then given to the UCSF Functional Genomics Core for quality control testing, single-end 50-bp RNA-Seq library preparation (Universal Plus mRNA kit, Nugen), and sequencing on an Illumina HiSeq 4000 system. Sequencing provided 1.034 billion total reads for the 28 samples, with an average of 853 millions of these reads aligning uniquely to the mouse genome (mm10/GRCm38.96). Alignment was performed using the Splice-aware STAR aligner STAR_2.7.2b. Reads uniquely mapped to known mRNAs were used to identify genes with differential expression between B6 and *Il33*$^{-/-}$ samples using the DESeq2 R package v1.24.0. Each tissue layer was analyzed independently, and Cooke's cutoff was applied to exclude outliers. We only analyzed protein coding genes for which at least two samples of the nine total per tissue layer had RPKMs greater than 30 (average RPKM for *Actb* was ~90,000, 198,000, and 179,000 in the decidua, myo/endo and mesometrial triangle, respectively).

For qRT-PCR analyses, cDNA was synthesized from 1 μg RNA using an iScript cDNA Synthesis Kit (Bio-Rad). The PCR reaction was performed with Evagreen dye (Biotium) using a CFX Connect Real-Time PCR Detection System (Bio-Rad). Primers are listed in Supplemental Table 2.

Prostaglandin measurements—Dissected uterine tissues were snap frozen and stored at −80°C before further processing. They were then weighed and pulverized in liquid nitrogen. The lipids were extracted with 500 μl ice-cold methanol-chloroform mixture (1:2) containing 10 μM indomethacin. A volume corresponding to 10 mg of tissue was taken and methanol was added to a final volume of 1 ml. These samples were sonicated 3 times (7 seconds each) and then vortexed. 100 μl was then dried in a speed vac and resuspend in PBS to quantify protein amounts using the Bradford assay (Abcam). The remaining 900 μl was centrifuged for 15 min at 10,000x*g* at 4°C to pellet precipitated proteins. The supernatants were kept at −80°C overnight to precipitate any additional proteins, and then evaporated in a speed vac. The samples were than resuspended in ELISA buffer, and concentrations of

PGE_2, PGE metabolites, $PGF_{2\alpha}$, and PGD_2 were determined using commercial ELISA kits (Cayman Chemical) following the manufacturer's instructions.

Statistics and reproducibility—The number of independent biological replicates and specific test employed for each experiment is shown in the figure or stated in the figure legend. Except for the RNA-Seq, statistical analyses were performed using Prism 9 (GraphPad). $p<0.05$ was considered to be statistically significant. Student's *t*-tests and Mann-Whitney *U* tests were unpaired and two-tailed. For the analysis of labor onset timing, a log-rank test was applied to all groups within an experiment to determine the overall *p* value shown in the figure; comparisons between pairs of groups were then calculated and considered to be significant if their *p* value was less than the Bonferroni-adjusted threshold *p* value calculated using the total number of meaningful comparisons within the experiment. The analysis of qRT-PCR data was performed on delta CT values.

Supplementary Material

Refer to Web version on PubMed Central for supplementary material.

ACKNOWLEDGMENTS

We thank Zhi-En Wang for performing cell sorting, Sofía Bustamante Eguiguren for assistance with the histology, Walter Eckalbar for assistance with the RNA-Seq analysis, and Gabrielle Rizzuto for comments on the manuscript. The graphical abstract was created in BioRender.com. Supported by NIH-NIAID R01AI150191 to A.E.

REFERENCES

1. Rokas A, Mesiano S, Tamam O, LaBella A, Zhang G, and Muglia L (2020). Developing a theoretical evolutionary framework to solve the mystery of parturition initiation. Elife 9. 10.7554/eLife.58343.
2. Mesiano S, DeFranco E, and Muglia LJ (2015). Chapter 42. Parturition. Plant TM, Zeleznik AJ, eds. In: Knobil and Neill's Physiology of Reproduction 4th Edition 2015; 1875–1955. Elsevier Inc. ed.
3. Romero R, Dey SK, and Fisher SJ (2014). Preterm labor: one syndrome, many causes. Science 345, 760–765. 10.1126/science.1251816. [PubMed: 25124429]
4. Nancy P, Siewiera J, Rizzuto G, Tagliani E, Osokine I, Manandhar P, Dolgalev I, Clementi C, Tsirigos A, and Erlebacher A (2018). H3K27me3 dynamics dictate evolving uterine states in pregnancy and parturition. J Clin Invest 128, 233–247. 10.1172/JCI95937. [PubMed: 29202469]
5. Kokubu K, Hondo E, Sakaguchi N, Sagara E, and Kiso Y (2005). Differentiation and elimination of uterine natural killer cells in delayed implantation and parturition mice. J Reprod Dev 51, 773–776. 10.1262/jrd.17033. [PubMed: 16127246]
6. Shynlova O, Nadeem L, Zhang J, Dunk C, and Lye S (2020). Myometrial activation: Novel concepts underlying labor. Placenta 92, 28–36. 10.1016/j.placenta.2020.02.005. [PubMed: 32056784]
7. Norwitz ER, Bonney EA, Snegovskikh VV, Williams MA, Phillippe M, Park JS, and Abrahams VM (2015). Molecular Regulation of Parturition: The Role of the Decidual Clock. Cold Spring Harb Perspect Med 5. 10.1101/cshperspect.a023143.
8. Ratajczak CK, and Muglia LJ (2008). Insights into parturition biology from genetically altered mice. Pediatr Res 64, 581–589. 10.1203/PDR.0b013e31818718d2. [PubMed: 18679156]
9. Cayrol C, and Girard JP (2018). Interleukin-33 (IL-33): A nuclear cytokine from the IL-1 family. Immunol Rev 281, 154–168. 10.1111/imr.12619. [PubMed: 29247993]
10. Allen JE, and Sutherland TE (2014). Host protective roles of type 2 immunity: parasite killing and tissue repair, flip sides of the same coin. Semin Immunol 26, 329–340. 10.1016/j.smim.2014.06.003. [PubMed: 25028340]

11. Markiewicz L, and Gurpide E (1994). Estrogenic and progestagenic activities coexisting in steroidal drugs: quantitative evaluation by in vitro bioassays with human cells. J Steroid Biochem Mol Biol 48, 89–94. 10.1016/0960-0760(94)90254-2. [PubMed: 8136310]
12. Terakawa J, Watanabe T, Obara R, Sugiyama M, Inoue N, Ohmori Y, Hosaka YZ, and Hondo E (2012). The complete control of murine pregnancy from embryo implantation to parturition. Reproduction 143, 411–415. 10.1530/REP-11-0288. [PubMed: 22198945]
13. Word RA, Li XH, Hnat M, and Carrick K (2007). Dynamics of cervical remodeling during pregnancy and parturition: mechanisms and current concepts. Semin Reprod Med 25, 69–79. 10.1055/s-2006-956777. [PubMed: 17205425]
14. Döring B, Shynlova O, Tsui P, Eckardt D, Janssen-Bienhold U, Hofmann F, Feil S, Feil R, Lye SJ, and Willecke K (2006). Ablation of connexin43 in uterine smooth muscle cells of the mouse causes delayed parturition. J Cell Sci 119, 1715–1722. 10.1242/jcs.02892. [PubMed: 16595547]
15. Vainchtein ID, Chin G, Cho FS, Kelley KW, Miller JG, Chien EC, Liddelow SA, Nguyen PT, Nakao-Inoue H, Dorman LC, et al. (2018). Astrocyte-derived interleukin-33 promotes microglial synapse engulfment and neural circuit development. Science 359, 1269–1273. 10.1126/science.aal3589. [PubMed: 29420261]
16. Dahlgren MW, Jones SW, Cautivo KM, Dubinin A, Ortiz-Carpena JF, Farhat S, Yu KS, Lee K, Wang C, Molofsky AV, et al. (2019). Adventitial Stromal Cells Define Group 2 Innate Lymphoid Cell Tissue Niches. Immunity 50, 707–722.e706. 10.1016/j.immuni.2019.02.002. [PubMed: 30824323]
17. Soyal SM, Mukherjee A, Lee KY, Li J, Li H, DeMayo FJ, and Lydon JP (2005). Cre-mediated recombination in cell lineages that express the progesterone receptor. Genesis 41, 58–66. 10.1002/gene.20098. [PubMed: 15682389]
18. Doisne JM, Balmas E, Boulenouar S, Gaynor LM, Kieckbusch J, Gardner L, Hawkes DA, Barbara CF, Sharkey AM, Brady HJ, et al. (2015). Composition, Development, and Function of Uterine Innate Lymphoid Cells. J Immunol 195, 3937–3945. 10.4049/jimmunol.1500689. [PubMed: 26371244]
19. Liu B, Yang J, Luo W, Zhang Y, Li J, Li H, Chen L, and Zhou Y (2017). Prostaglandin D 2 is the major cyclooxygenase-1-derived product in prepartum mouse uteri where it mediates an enhanced in vitro myometrial contraction. Eur J Pharmacol 813, 140–146. 10.1016/j.ejphar.2017.08.015. [PubMed: 28822852]
20. Herington JL, O'Brien C, Robuck MF, Lei W, Brown N, Slaughter JC, Paria BC, Mahadevan-Jansen A, and Reese J (2018). Prostaglandin-Endoperoxide Synthase 1 Mediates the Timing of Parturition in Mice Despite Unhindered Uterine Contractility. Endocrinology 159, 490–505. 10.1210/en.2017-00647. [PubMed: 29029054]
21. Gross GA, Imamura T, Luedke C, Vogt SK, Olson LM, Nelson DM, Sadovsky Y, and Muglia LJ (1998). Opposing actions of prostaglandins and oxytocin determine the onset of murine labor. Proc Natl Acad Sci U S A 95, 11875–11879. 10.1073/pnas.95.20.11875. [PubMed: 9751758]
22. Gross G, Imamura T, Vogt SK, Wozniak DF, Nelson DM, Sadovsky Y, and Muglia LJ (2000). Inhibition of cyclooxygenase-2 prevents inflammation-mediated preterm labor in the mouse. Am J Physiol Regul Integr Comp Physiol 278, R1415–1423. 10.1152/ajpregu.2000.278.6.R1415. [PubMed: 10848506]
23. Tsuboi K, Iwane A, Nakazawa S, Sugimoto Y, and Ichikawa A (2003). Role of prostaglandin H2 synthase 2 in murine parturition: study on ovariectomy-induced parturition in prostaglandin F receptor-deficient mice. Biol Reprod 69, 195–201. 10.1095/biolreprod.102.013870. [PubMed: 12620936]
24. Johnston LK, Hsu CL, Krier-Burris RA, Chhiba KD, Chien KB, McKenzie A, Berdnikovs S, and Bryce PJ (2016). IL-33 Precedes IL-5 in Regulating Eosinophil Commitment and Is Required for Eosinophil Homeostasis. J Immunol 197, 3445–3453. 10.4049/jimmunol.1600611. [PubMed: 27683753]
25. Fettrelet T, Gigon L, Karaulov A, Yousefi S, and Simon HU (2021). The Enigma of Eosinophil Degranulation. Int J Mol Sci 22. 10.3390/ijms22137091.
26. Carlens J, Wahl B, Ballmaier M, Bulfone-Paus S, Förster R, and Pabst O (2009). Common gamma-chain-dependent signals confer selective survival of eosinophils in the murine small intestine. J Immunol 183, 5600–5607. 10.4049/jimmunol.0801581. [PubMed: 19843944]

27. Tagliani E, Shi C, Nancy P, Tay CS, Pamer EG, and Erlebacher A (2011). Coordinate regulation of tissue macrophage and dendritic cell population dynamics by CSF-1. J Exp Med 208, 1901–1916. 10.1084/jem.20110866. [PubMed: 21825019]
28. Gouon-Evans V, and Pollard JW (2001). Eotaxin is required for eosinophil homing into the stroma of the pubertal and cycling uterus. Endocrinology 142, 4515–4521. 10.1210/endo.142.10.8459. [PubMed: 11564717]
29. Diener KR, Robertson SA, Hayball JD, and Lousberg EL (2016). Multi-parameter flow cytometric analysis of uterine immune cell fluctuations over the murine estrous cycle. J Reprod Immunol 113, 61–67. 10.1016/j.jri.2015.11.005. [PubMed: 26759962]
30. Kopf M, Brombacher F, Hodgkin PD, Ramsay AJ, Milbourne EA, Dai WJ, Ovington KS, Behm CA, Köhler G, Young IG, and Matthaei KI (1996). IL-5-deficient mice have a developmental defect in CD5+ B-1 cells and lack eosinophilia but have normal antibody and cytotoxic T cell responses. Immunity 4, 15–24. 10.1016/s1074-7613(00)80294-0. [PubMed: 8574848]
31. Park YM, and Bochner BS (2010). Eosinophil survival and apoptosis in health and disease. Allergy Asthma Immunol Res 2, 87–101. 10.4168/aair.2010.2.2.87. [PubMed: 20358022]
32. Robertson SA, Mau VJ, Young IG, and Matthaei KI (2000). Uterine eosinophils and reproductive performance in interleukin 5-deficient mice. J Reprod Fertil 120, 423–432. 10.1530/jrf.0.1200423. [PubMed: 11058459]
33. Dougan M, Dranoff G, and Dougan SK (2019). GM-CSF, IL-3, and IL-5 Family of Cytokines: Regulators of Inflammation. Immunity 50, 796–811. 10.1016/j.immuni.2019.03.022. [PubMed: 30995500]
34. Grimaldi JC, Yu NX, Grunig G, Seymour BW, Cottrez F, Robinson DS, Hosken N, Ferlin WG, Wu X, Soto H, et al. (1999). Depletion of eosinophils in mice through the use of antibodies specific for C-C chemokine receptor 3 (CCR3). J Leukoc Biol 65, 846–853. 10.1002/jlb.65.6.846. [PubMed: 10380909]
35. Menzies FM, Higgins CA, Shepherd MC, Nibbs RJ, and Nelson SM (2012). Mast cells reside in myometrium and cervix, but are dispensable in mice for successful pregnancy and labor. Immunol Cell Biol 90, 321–329. 10.1038/icb.2011.40. [PubMed: 21577230]
36. Lloyd CM, and Snelgrove RJ (2018). Type 2 immunity: Expanding our view. Sci Immunol 3. 10.1126/sciimmunol.aat1604.
37. Kakkar R, Hei H, Dobner S, and Lee RT (2012). Interleukin 33 as a mechanically responsive cytokine secreted by living cells. J Biol Chem 287, 6941–6948. 10.1074/jbc.M111.298703. [PubMed: 22215666]
38. Domingo C, Palomares O, Sandham DA, Erpenbeck VJ, and Altman P (2018). The prostaglandin D2receptor 2 pathwayin asthma: a key player in airwayinflammation. Respir Res 19, 189. 10.1186/s12931-018-0893-x. [PubMed: 30268119]
39. Crankshaw DJ, and Gaspar V (1992). Effects of prostanoids on the rat's myometrium in vitro during pregnancy. Biol Reprod 46, 392–400. 10.1095/biolreprod46.3.392. [PubMed: 1377509]
40. Gaynor LM, and Colucci F (2017). Uterine Natural Killer Cells: Functional Distinctions and Influence on Pregnancy in Humans and Mice. Front Immunol 8, 467. 10.3389/fimmu.2017.00467. [PubMed: 28484462]
41. Lutton EJ, Lammers WJEP, James S, van den Berg HA, and Blanks AM (2018). Identification of uterine pacemaker regions at the myometrial-placental interface in the rat. J Physiol 596, 2841–2852. 10.1113/JP275688. [PubMed: 29704394]
42. Valero-Pacheco N, Tang EK, Massri N, Loia R, Chemerinski A, Wu T, Begum S, El-Naccache DW, Gause WC, Arora R, et al. (2022). Maternal IL-33 critically regulates tissue remodeling and type 2 immune responses in the uterus during early pregnancy in mice. Proc Natl Acad Sci U S A 119, e2123267119. 10.1073/pnas.2123267119. [PubMed: 35994660]
43. Stelzer IA, Ghaemi MS, Han X, Ando K, Hédou JJ, Feyaerts D, Peterson LS, Rumer KK, Tsai ES, Ganio EA, et al. (2021). Integrated trajectories of the maternal metabolome, proteome, and immunome predict labor onset. Sci Transl Med 13. 10.1126/scitranslmed.abd9898.
44. Huang B, Faucette AN, Pawlitz MD, Pei B, Goyert JW, Zhou JZ, El-Hage NG, Deng J, Lin J, Yao F, et al. (2017). Interleukin-33-induced expression of PIBF1 by decidual B cells protects against preterm labor. Nat Med 23, 128–135. 10.1038/nm.4244. [PubMed: 27918564]

45. Griesenauer B, and Paczesny S (2017). The ST2/IL-33 Axis in Immune Cells during Inflammatory Diseases. Front Immunol 8, 475. 10.3389/fimmu.2017.00475. [PubMed: 28484466]
46. Xu Y, Romero R, Miller D, Silva P, Panaitescu B, Theis KR, Arif A, Hassan SS, and Gomez-Lopez N (2018). Innate lymphoid cells at the human maternal-fetal interface in spontaneous preterm labor. Am J Reprod Immunol 79, e12820. 10.1111/aji.12820. [PubMed: 29457302]
47. Mendes J, Rodrigues-Santos P, Areia AL, Almeida JS, Alves V, Santos-Rosa M, and Mota-Pinto A (2021). Type 2 and type 3 innate lymphoid cells at the maternal-fetal interface: implications in preterm birth. BMC Immunol 22, 28. 10.1186/s12865-021-00423-x. [PubMed: 33957866]
48. Romero R, Kusanovic JP, Muñoz H, Gomez R, Lamont RF, and Yeo L (2010). Allergy-induced preterm labor after the ingestion of shellfish. J Matern Fetal Neonatal Med 23, 351–359. 10.3109/14767050903177193. [PubMed: 19900031]
49. Romero R, Kusanovic JP, Gomez R, Lamont R, Bytautiene E, Garfield RE, Mittal P, Hassan SS, and Yeo L (2010). The clinical significance of eosinophils in the amniotic fluid in preterm labor. J Matern Fetal Neonatal Med 23, 320–329. 10.3109/14767050903168465. [PubMed: 19900034]
50. Bytautiene E, Romero R, Vedernikov YP, El-Zeky F, Saade GR, and Garfield RE (2004). Induction of premature labor and delivery by allergic reaction and prevention by histamine H1 receptor antagonist. Am J Obstet Gynecol 191, 1356–1361. 10.1016/j.ajog.2004.06.092. [PubMed: 15507965]
51. Pichery M, Mirey E, Mercier P, Lefrancais E, Dujardin A, Ortega N, and Girard JP (2012). Endogenous IL-33 is highly expressed in mouse epithelial barrier tissues, lymphoid organs, brain, embryos, and inflamed tissues: in situ analysis using a novel Il-33-LacZ gene trap reporter strain. J Immunol 188, 3488–3495. 10.4049/jimmunol.1101977. [PubMed: 22371395]
52. Nussbaum JC, Van Dyken SJ, von Moltke J, Cheng LE, Mohapatra A, Molofsky AB, Thornton EE, Krummel MF, Chawla A, Liang HE, and Locksley RM (2013). Type 2 innate lymphoid cells control eosinophil homeostasis. Nature 502, 245–248. 10.1038/nature12526. [PubMed: 24037376]
53. Chen WY, Hong J, Gannon J, Kakkar R, and Lee RT (2015). Myocardial pressure overload induces systemic inflammation through endothelial cell IL-33. Proc Natl Acad Sci U S A 112, 7249–7254. 10.1073/pnas.1424236112. [PubMed: 25941360]
54. Nancy P, Tagliani E, Tay CS, Asp P, Levy DE, and Erlebacher A (2012). Chemokine gene silencing in decidual stromal cells limits T cell access to the maternal-fetal interface. Science 336, 1317–1321. 10.1126/science.1220030. [PubMed: 22679098]

Highlights

1. Progestin administration establishes a uterus-intrinsic model of parturition in mice
2. Parturition is delayed in progestin-treated IL-33- and IL-5-deficient mice
3. Uterine fibroblasts are a key IL-33 source driving parturition
4. Innate type 2 immune activity increases in the uterus prior to labor onset

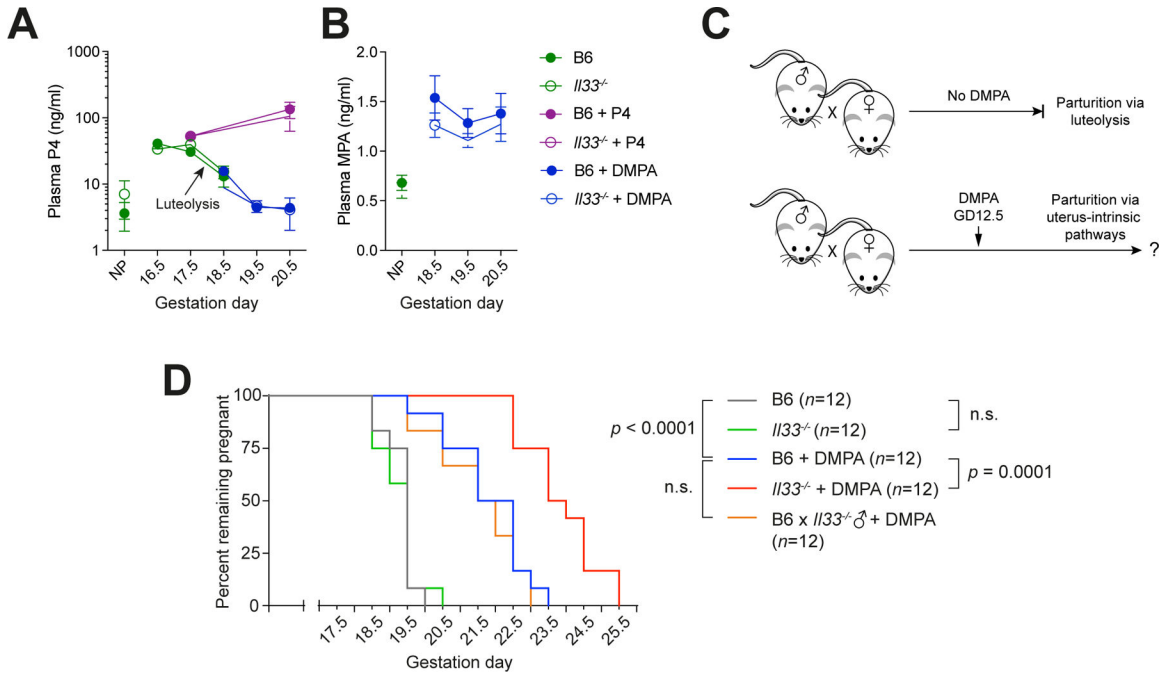

Figure 1. IL-33 deficiency delays labor onset in mice when parturition occurs through uterus-intrinsic pathways.

(**A**) Late gestation plasma P4 concentrations, assessed by ELISA, in untreated mice, mice injected daily with 2 mg P4 starting on GD16.5, and mice injected once on GD12.5 with 250 μg DMPA. Untreated, NP mice are also shown. *n*=3–6 mice/group; mean+/−SEM. (**B**) Late gestation plasma MPA concentrations, assessed by ELISA, in mice injected with DMPA on GD12.5 (*n*=6 mice/group; mean+/-SEM). Data for NP mice demonstrate the ELISA background (*n*=3 mice/group). (**C**) Schematic of parturition timing experiments. In the absence of DMPA administration, mice enter labor on ~GD19.5 as the result of luteolysis. DMPA administration, which extends gestation length, allows for the evaluation of uterus-intrinsic parturition pathways. Maintaining pregnancy this way causes 100% fetal demise by GD22.5, presumably due to fetal overgrowth or uterine contraction against a closed cervix (e.g., Figure S1A). (**D**) Parturition timing in *Il33*$^{-/-}$ and control B6 mice that were either untreated or injected with DMPA on GD12.5. Groups were compared by the log-rank test. Females were mated with B6 males unless otherwise indicated. See also Figure S1.

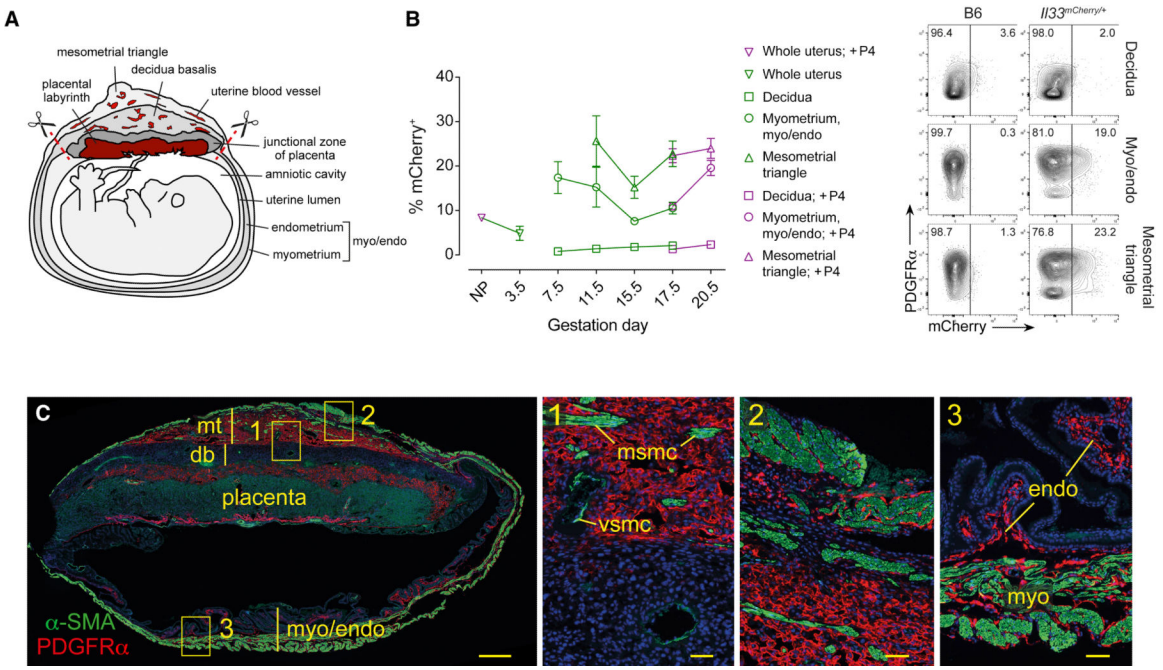

Figure 2. Myo/endo and mesometrial triangle PDGFRα+ stromal cells are the main sources of IL-33 in the pregnant uterus.

(**A**) Schematic of an implantation site on ~GD13.5. Red dashed lines show where we separate the mesometrial triangle from the myo/endo. (**B**) Percent IL-33mCherry positivity among stromal ($CD45^{-}$ $ICAM2^{-}$ $EpCAM^{-}$) cells of the NP and pregnant uterus in *Il33*$^{mCherry/+}$ mice, as determined by flow cytometry (n=5 mice/group; mean+/−SEM; see Figure S2A for gating). Representative contour plots with PDGFRα co-staining (n=5 mice/group collected over 2–3 independent experiments per genotype) are shown for mice on GD20.5; Figure S3A shows plots for all time points. The mCherry gate was placed so that less than 1% of the stromal cells in B6 mice on GD17.5 were $mCherry^{+}$. P4 was given to non-pregnant mice to establish a pregnancy-like endocrine state. (**C**) PDGFRα immunostaining of an GD18.5 implantation site, with bracketed areas shown in close-up (representative of n=4 B6 mice). The embryo was removed before fixation. α-smooth muscle actin (α-SMA) identifies SMCs. db, decidua basalis; mt, mesometrial triangle; myo, myometrium; endo, endometrium. Note that the mesometrial triangle contains both vascular SMCs (vsmc) and myometrial SMC bundles (msmc), which are characteristically dispersed at this anatomic location. Scale bars: 500 μm (left panel); 50 μm (three right panels). See also Figures S2 and S3.

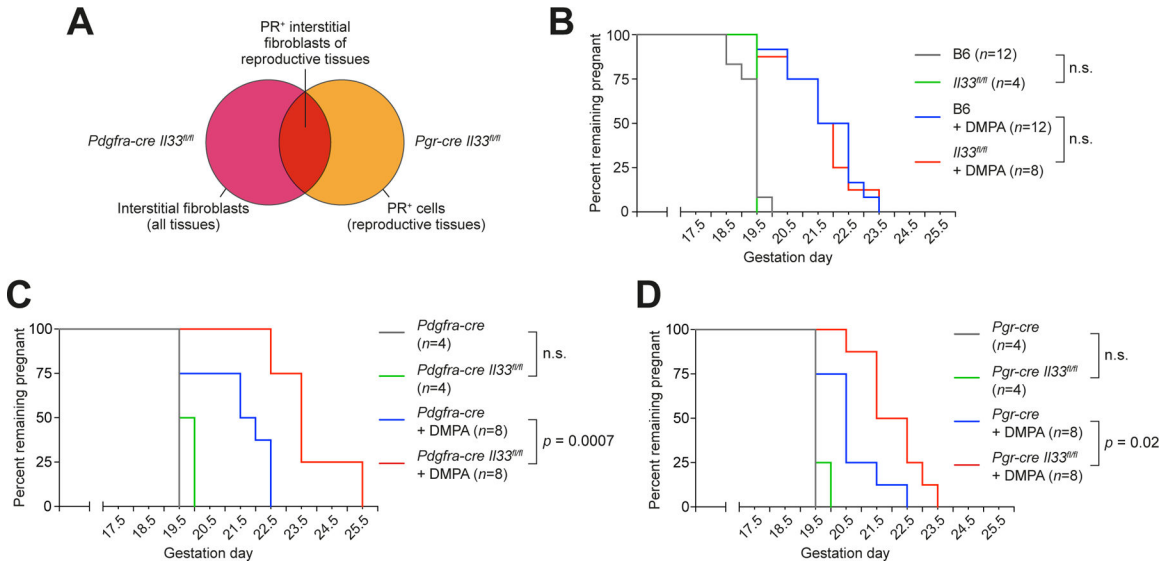

Figure 3. Cell type-specific requirements for *Il33* expression in parturition.

(**A**) Schematic of cell types targeted for *Il33* deletion. The *Pdgfra-cre* experiment used mice hemizygous for a *Pdgfra-cre* transgene and the *Pgr-cre* experiment used mice heterozygous for a *Pgr* allele bearing a targeted *cre* construct. Targeted cells common to both experiments are interstitial fibroblasts of reproductive organs, including the uterus. (**B-D**) Parturition timing. Where indicated, mice were injected with DMPA on GD12.5. B6 mice are the same as in Figure 1D. Groups were compared by the log-rank test. See also Figure S4.

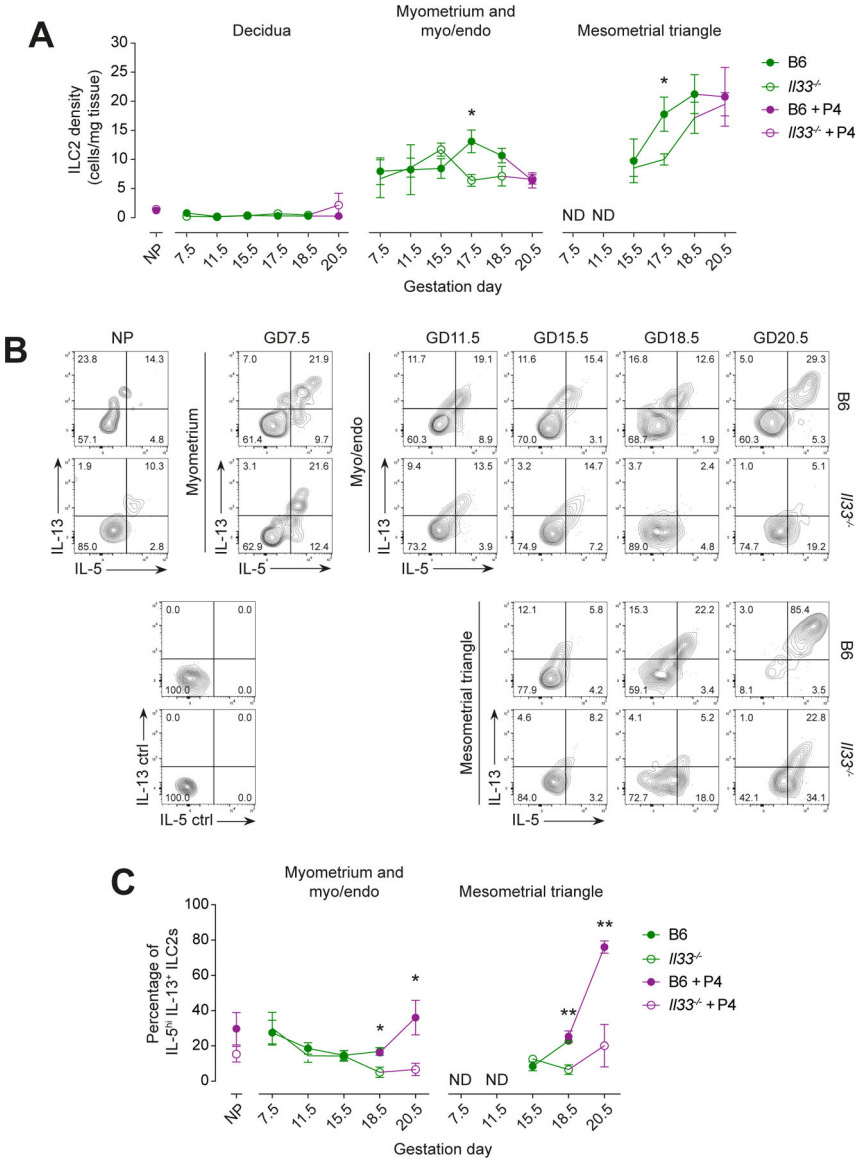

Figure 4. IL-33-dependent uterine ILC2 expansion and activation shortly before labor onset.

Where indicated, mice were given daily P4 injections starting on GD16.5 to extend gestation to GD20.5, or starting on GD14.5 prior to sacrifice on GD18.5 to assess the effects of P4 injection per se. (**A**) ILC2 tissue densities in whole NP uteri and dissected uterine tissue layers of B6 and *Il33*$^{-/-}$ mice, as determined by flow cytometry. *, p<0.05 by Student's t-test (n=6 mice/group; mean+/-SEM). ND, not determined. (**B, C**) IL-5 and IL-13 production by uterine ILC2s. Uterine cell suspensions were stimulated ex vivo with PMA/ionomycin, and IL-5/13 expression was assessed by intracellular staining. Panel B shows representative contour plots (n=4 mice/group collected over 2–5 independent experiments per time point), including isotype control (ctrl) staining for the GD18.5 mesometrial triangle; panel C shows quantified percentages of IL-5^{hi} IL-13^{+} ILC2s. *, p<0.05; **, p<0.01 by Student's t-test (n=4 mice/group; mean+/−SEM). See also Figure S5.

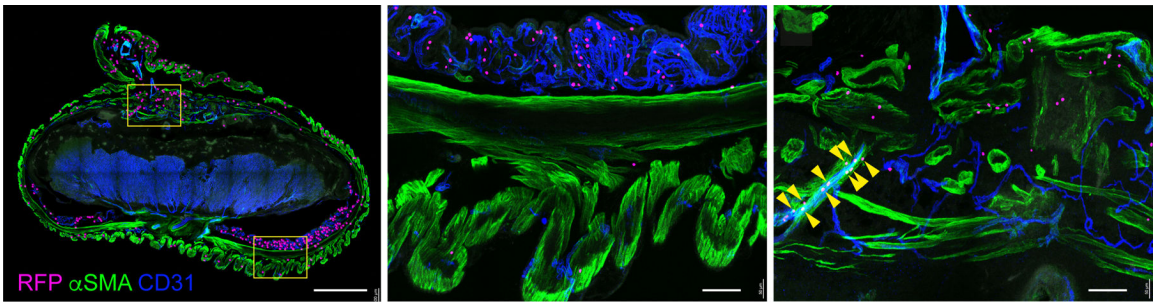

Figure 5. Distribution of ILC2s in the late gestation uterus.

Anti-RFP immunofluorescence was performed on 300 μm sections of GD17.5 implantation sites from *Il5-cre*R26RFP mice, in which *Il5-cre*-mediated recombination induces high, permanent, RFP (tdTomato) expression in ILC2s and rare T cells. Embryos were removed before fixation. The sections were co-stained with antibodies to α-SMA and CD31 to visualize SMCs and endothelial cells, respectively. RFP^+ cells were artificially surfaced in (**A**) so that they would be evident in the panoramic view. Note the RFP^+ cells associated with myometrial SMC bundles and vascular structures, including an arteriole coated with vascular SMCs (**C**; arrowheads). Data are representative of n=4 mice. Scale bars: 1 μm (**A**); 100 μm (**B, C**).

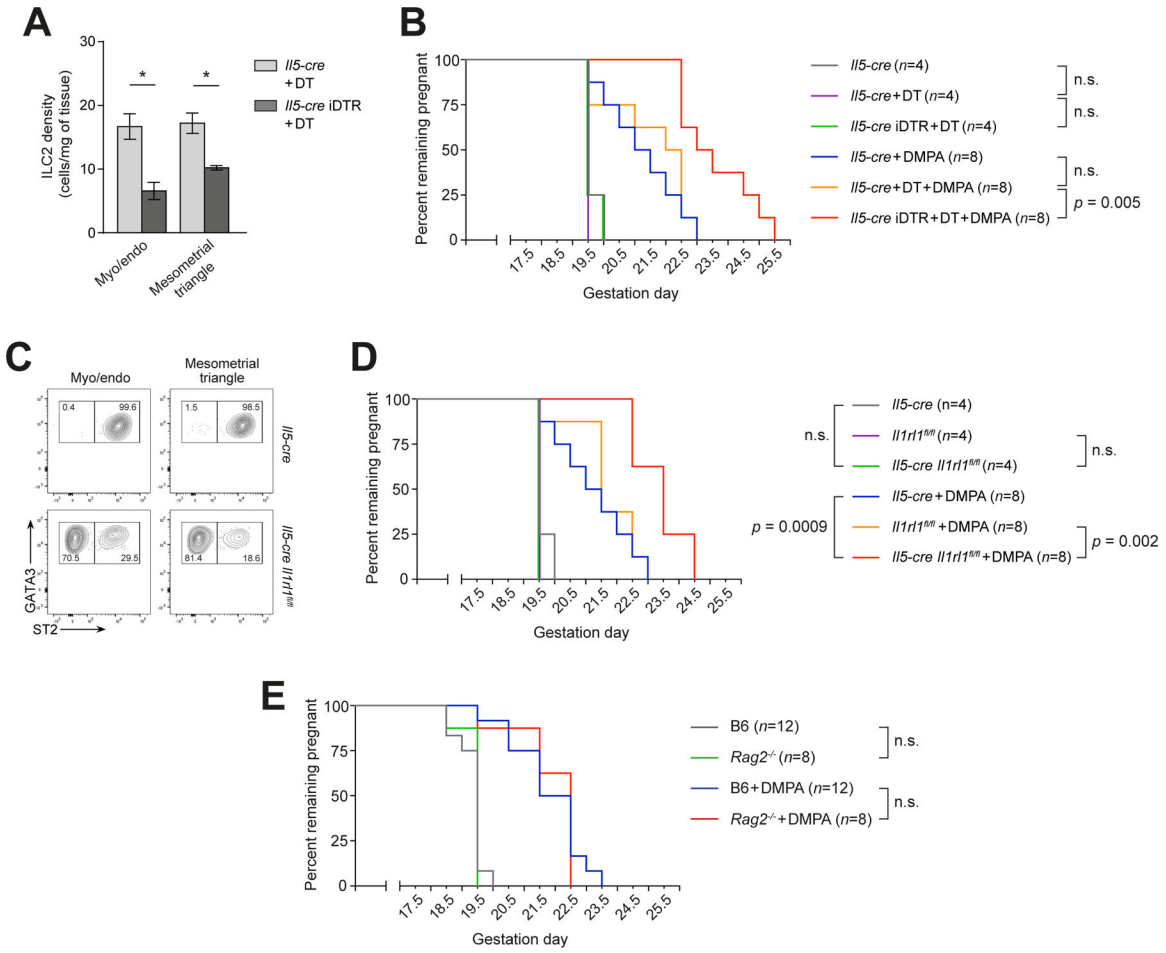

Figure 6. Delayed labor onset in mice with depleted or IL-33-unresponsive ILC2s.

For parturition timing experiments, mice were injected as indicated with a single dose of DMPA on GD12.5. Groups were compared by the log-rank test. (**A**) Extent of ILC2 depletion in *Il5-cre* iDTR and control *Il5-cre* mice given DT every other day as indicated starting on GD12.5 and sacrificed on GD18.5. *, $p<0.05$ by Student's *t*-test ($n=4$ mice/group; mean+/-SEM). (**B**) Parturition timing in such ILC2-depleted mice. (**C**) ST2 expression by uterine ILC2s in *Il5-cre Il1rl1*$^{f/f}$ and control *Il5-cre* mice (representative contour plots from GD18.5; $n=3$/group collected over 3 independent experiments). (**D**) Parturition timing in *Il5-cre Il1rl1*$^{f/f}$ mice. (**E**) Parturition timing in *Rag2*$^{-/-}$ mice. B6 mice are the same as in Figure 1D.

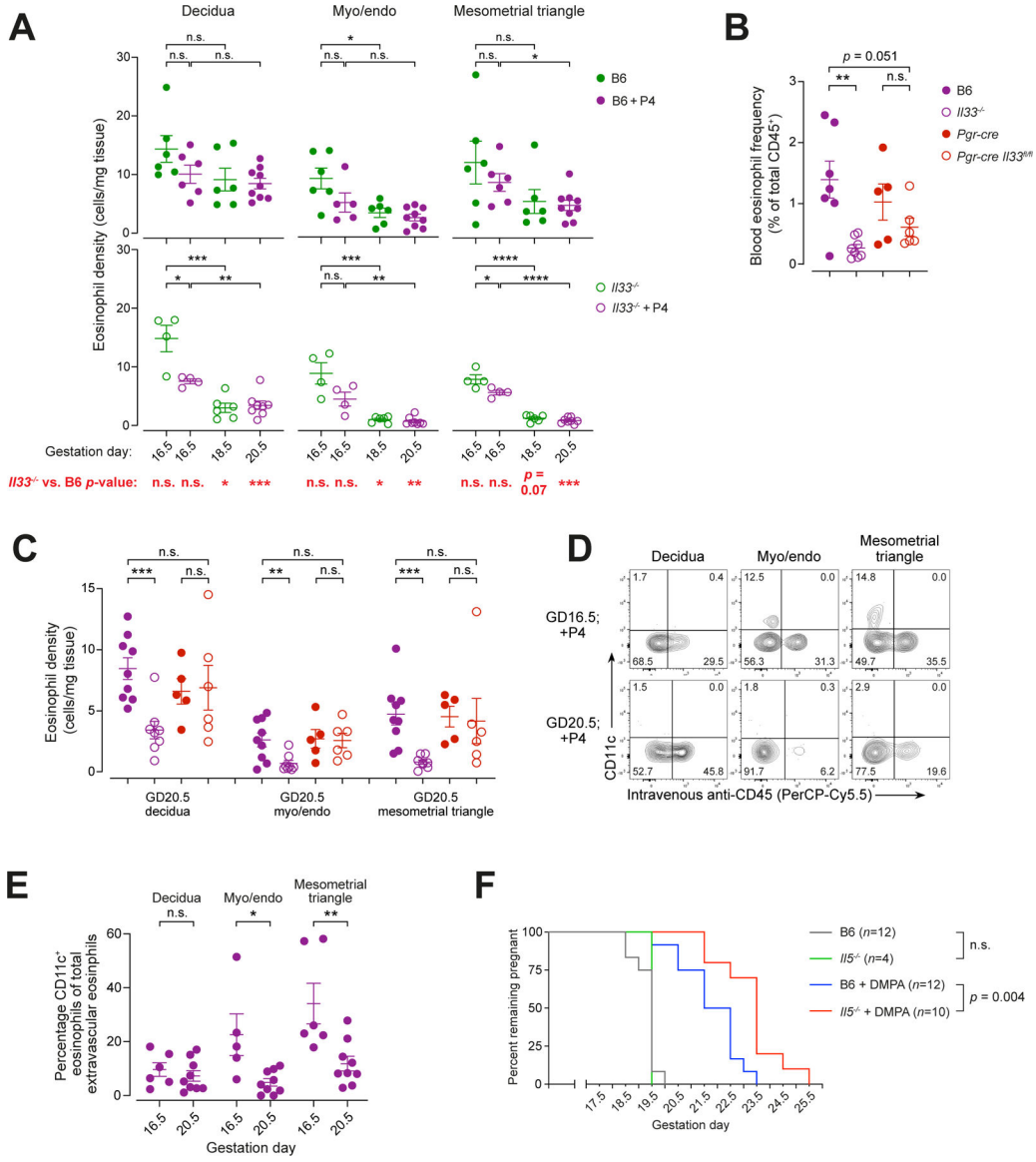

Figure 7. Eosinophil dynamics in the prepartum uterus and delayed labor onset in IL-5-deficient mice.

(A-E) Analysis of uterine densities, blood frequencies, and CD11c expression by eosinophils in late gestation. See Figure S5D for gating. Mice were intravenously injected 5 minutes before sacrifice with PerCP-Cy5.5-conjugated anti-CD45 antibodies. Only extravascular cells were used to calculate tissue densities. Mice sacrificed on GD20.5 were injected daily with P4 starting on GD16.5; where indicated some mice sacrificed on GD16.5 were injected daily with P4 starting on GD12.5. All graphs show data for individual mice and mean+/-SEM. *, $p<0.05$; **, $p<0.01$; ***, $p<0.001$; ****, $p<0.0001$ by Student's t-test. (**A**) Eosinophil tissue densities in the prepartum uterus. (**B**) Blood eosinophil frequencies on GD20.5. (**C**) Uterine eosinophil densities on GD20.5. B6 and *Il33*$^{-/-}$ data are the same as in Panel A. (**D, E**) CD11c expression by uterine eosinophils in B6 mice (representative contour plots from n=6–9 mice/group collected over 5 independent experiments per time point, and

summary data, respectively). (**F**) Parturition timing in *Il5*$^{-/-}$ mice. Groups were compared by the log-rank test. B6 mice are the same as in Figure 1D. See also Figures S5 and S6.

KEY RESOURCES TABLE

REAGENT or RESOURCE	SOURCE	IDENTIFIER
Antibodies		
Anti-mouse CD45 PerCPCy5.5 (clone 30-F11)	BD Biosciences	Cat#550994; RRID: AB 394003
Anti-mouse CD45 BUV395 (clone 30-F11)	BD Biosciences	Cat#564279; RRID: AB 2651134
Anti-mouse CD4 BV711 (clone RM4–5)	BioLegend	Cat#100549; RRID: AB 11219396
Anti-mouse/human CD11b BV605 (clone M1/70)	BioLegend	Cat#101237; RRID: AB 11126744
Anti-mouse NK1.1 APC-Cy7 (clone PK136)	BioLegend	Cat#108723; RRID: AB 830870
Anti-mouse CD19 PE/Dazzle 594 (clone 6D5)	BioLegend	Cat#115553; RRID: AB 2564000
Anti-mouse CD90.2 (Thy-1.2) BV421 (clone 53–2.1)	BioLegend	Cat#140327; RRID: AB 2686992
Anti-mouse CD3 Alexa Fluor 700 (clone 17A2)	BioLegend	Cat#100216; RRID: AB 493697
Anti-mouse T1/ST2 PE (clone DJ8)	MDbioproducts	Cat#101001PE
Anti-human/mouse GATA3 eFluor660 (clone TWAJ)	Invitrogen	Cat#50–9966-42; RRID: AB 10596663
Anti-mouse FOXP3 PECy7 (clone FJK-16s)	Invitrogen	Cat#25–5773-82; RRID: AB 891552
Anti-mouse IL-13 PECy7 (clone eBio13A)	Invitrogen	Cat#25–7133-80; RRID: AB 2573529
Anti-mouse/human IL-5 (clone TRFK5)	BioLegend	Cat#504301; RRID: AB 315325
Anti-rat IgG1 FITC (clone MRG1–58)	BioLegend	Cat#407405; RRID: AB 492921
Anti-mouse CD102 (ICAM-2) FITC (clone 3C4)	BioLegend	Cat#105606; RRID: AB 313199
Anti-mouse CD326 (Ep-CAM) PECy7 (clone G8.8)	BioLegend	Cat#118215; RRID: AB 1236477
Anti-mouse CD326 (Ep-CAM) BV711 (clone G8.8)	BioLegend	Cat#118233; RRID:AB 2632775
Anti-mouse CD140a (PDGFRα) APC (clone APA5)	BioLegend	Cat#135907; RRID: AB 2043969
Anti-mouse CD140a (PDGFRα) PE (clone APA5)	BioLegend	Cat#135905; RRID AB 1953268
Anti-mouse gp38/Podoplanin APC-Cy7 (clone8.1.1)	BioLegend	Cat#127417; RRID: AB 2629803
Anti-mouse Ly-6A/E (Sca-1) BV711 (clone D7)	BioLegend	Cat#108131; RRID: AB 2562241
Anti-mouse CD54 (ICAM-1) PE (clone YN1/1.7.4)	BioLegend	Cat#116107; RRID: AB 313698
Anti-mouse Ly-6G APC (clone 1A8)	BioLegend	Cat#127614; RRID: AB_2227348
Anti-mouse F4/80 FITC (clone BM8)	BioLegend	Cat#123108; RRID: AB_893502
Anti-mouse Siglec-F BV421 (clone E50–2440)	BD Biosciences	Cat#562681; RRID: AB_2722581
Anti-mouse CD11c BV650 (clone N418)	BioLegend	Cat#117339; RRID: AB_2562414
Anti-mouse CCR3 (CD193) (clone 6S2–19-4)	Bio X Cell	Cat#BE0316; RRID:AB_2754554
Rat IgG2b isotype control (clone LTF-2)	Bio X Cell	Cat#BE0090; RRID:AB_1107780
Anti-mouse Alpha-Smooth Muscle Actin Alexa Fluor 488 (clone 1A4)	eBioscience	Cat#53–9760-82; RRID: AB 2574461
Anti-mouse Alpha-Smooth Muscle Actin Alexa Fluor 647 (clone 1A4)	Novus Biologicals	Cat#NBP2–34522AF647
Anti-mouse CD31 (clone MEC13.3)	BioLegend	Cat#102501; RRID:AB_312908
Anti-mouse PGFDR alpha (clone EPR22059–270)	Abcam	Cat#ab203491; RRID:AB_2892065
Anti-mouse COX-2 (clone D5H5)	Cell Signaling Technology	Cat#12282; RRID:AB_2571729
Living Colors anti-DsRed Rabbit Polyclonal Pan Antibody	Takara Bio	Cat#632496
(HRP-) conjugated donkey anti-rabbit IgG-secondary antibodies	Jackson ImmunoResearch	Cat#711–005-152; RRID: AB_2340585

REAGENT or RESOURCE	SOURCE	IDENTIFIER
Donkey anti-Rabbit IgG (H+L) Highly Cross-Adsorbed Secondary Antibody, Alexa Fluor Plus 555	Thermo Fisher Scientific	Cat#A32794; RRID:AB_2762834
Donkey Anti-Rat IgG H&L (Alexa Fluor® 647) preadsorbed	Abcam	Cat# ab150155; RRID:AB_2813835
Anti-FcgIII/II receptor antibodies (clone 2.4G2)	Bio X Cell	Cat#BE0307; RRID:AB_2736987
Chemicals, peptides, and recombinant proteins		
Ambion™ TRIzol™ Reagent	Thermo Fisher Scientific	Cat#15596026
Biotin-N-hydroxysuccinimide ester	Sigma-Aldrich	Cat#H1759–100MG; CAS: 35013–72-0
Bovine Serum Albumin	Sigma-Aldrich	Cat#A2153; CAS: 9048–46-8
Bradford Reagent	Abcam	Cat# ab119216
Brefeldin A (GolgiPlugTM)	BD Biosciences	Cat# 555029
Chloroform	Sigma-Aldrich	Cat# C2432–25ML; CAS: 67–66-3
Dapi-Fluoromount-G™	Electron Microscopy Sciences	Cat#17984–24
Depo-Provera (depot medroxyprogesterone acetate; DMPA)	Pfizer	Cat#0009–0746-30
Dimethyl sulfoxide	Sigma-Aldrich	Cat#D8418; CAS: 67–68-5
Diphtheria toxin	Calbiochem	Cat#D0564–1MG
dNTP Mix, 10mM each	Thermo Fisher Scientific	Cat# R0193
Donkey serum	EMD Millipore	Cat#S30–100ML
EDTA, 0.5 M pH 8.0	Corning	Cat#MT-46034CI
Ethanol, 200 proof (100%), USP, Decon™ Labs	Fisherscientific	Cat#22032601
EvaGreen® dye	Biotium	Cat#31000
Fixable Viability Dye eFluor™ 506	Invitrogen	Cat# 65–0866-14
Gibco™ RPMI 1640 Medium	Thermo Fisher Scientific	Cat#11–875-093
Glycine	Sigma-Aldrich	Cat#G8898; CAS: 56–40-6
Hanks' Balanced Salt Solution, 1X (HBSS)	Corning	Cat#21–023-CV
Ionomycin, calcium salt	AdipoGen Life Sciences	Cat#AG-CN2–0418-M001; CAS 56092–82-1
Liberase™ TL Research Grade	Sigma-Aldrich	Cat#05401020001
Methanol	Sigma-Aldrich	Cat#179337–4L; CAS: 67–56-1
Monensin	Abcam	Cat# ab193381
Paraformaldehyde	Sigma-Aldrich	Cat#158127; CAS: 30525–89-4
Phorbol 12-myristate 13-acetate (PMA)	AdipoGen Life Sciences	Cat#AG-CN2–0010-M001; CAS 16561–29-8
Progesterone	Sigma-Aldrich	Cat#P0130; CAS: 57–83-0
SC-236	Axon Medchem	Cat# 2108; CAS: 170569–86-5
Sesame seed oil	Sigma-Aldrich	Cat#S3547; CAS: 8008–74-0
Streptavidin, Alexa Fluor™ 594 conjugate	ThermoFisher Scientific	Cat#S11227
Triton TM X-100	Sigma-Aldrich	Cat#X100; CAS: 9002–93-1
Trypsin 2.5% (10X), no phenol red	Thermo Fisher Scientific	Cat#15090046
TSA® Blocking Reagent	PerkinElmer	Cat#FP1020
TWEEN® 20	Sigma-Aldrich	Cat#P1379; CAS: 9005–64-5

REAGENT or RESOURCE	SOURCE	IDENTIFIER
Tyramine	Sigma-Aldrich	Cat#T90344–5G; CAS: 51–67-2
Critical commercial assays		
Human Medroxyprogesterone Acetate (MPA) ELISA Kit	MyBioSource	Cat.No: MBS9349818
Progesterone ELISA Kit	Cayman Chemical	Cat#No. 582601
Prostaglandin $F_{2\alpha}$ ELISA Kit	Cayman Chemical	Cat# No. 516011
Prostaglandin D_2 ELISA Kit	Cayman Chemical	Cat# No. 512031
Prostaglandin E_2 ELISA Kit	Cayman Chemical	Cat# No. 514010
Prostaglandin E Metabolite ELISA Kit	Cayman Chemical	Cat# No. 514531
iScript TM cDNA Synthesis Kit	Bio-Rad	Cat#170–8891
eBioscience™ Foxp3 / Transcription Factor Staining Buffer Set	Invitrogen	Cat#00–5523-00
CountBright™ Absolute Counting Beads	Invitrogen	Cat#C36950
Deposited data		
RNA-Seq raw and analyzed data	This manuscript	GEO: GSE181904
Mouse reference genome GRCm38/mm10	Genome Browser Gateway	http://genome.ucsc.edu/cgi-bin/hgGateway
Experimental models: Organisms/strains		
Mouse: C57BL/6 (B6)	The Jackson Laboratory	RRID:IMSR_JAX:000664
Mouse: C57BL/6-Tg(Pdgfra-cre)1Clc/J (*Pdgfra-cre*)	The Jackson Laboratory	RRID:IMSR_JAX:013148
Mouse: C57BL/6-*Gt(ROSA)26Sor*$^{tm1(HBEGF)Awai}$/J (iDTR)	The Jackson Laboratory	RRID:IMSR_JAX:007900
Mouse: B6.Cg-*Rag2*$^{tm1.1Cgn}$/J (*Rag2*$^{-/-}$)	The Jackson Laboratory	RRID:IMSR_JAX:008449
Mouse: *Il33*$^{Gt/Gt}$(*Il33*$^{-/-}$)	Pichery et al., 2012	N/A
Mouse: B6(C)-*Il5*$^{tm1.1(icre)Lky}$/J (*Il5-cre*)	Nussbaum et al., 2013	RRID:IMSR_JAX:030926
Mouse: *Il33*$^{fl/fl}$	Chen et al., 2015	N/A
Mouse: *Il1rl1*$^{fl/fl}$	Chen et al., 2015	N/A
Mouse: B6.*Il33*$^{mCherry/mCherry}$ (IL-33mCherry)	Vainchtein et al., 2018	N/A
Mouse: *Il5-cre* B6.Cg-*Gt(ROSA)26Sor*$^{tm14(CAG-tdTomato)Hze}$/J (IL5CreR26RFP)	Dahlgren et al., 2019	RRID:IMSR_JAX:007914
Mouse: *Pgr-cre*	Soyal et al., 2005	N/A
Mouse: B6.129(Cg)-*Gt(ROSA)26Sor*$^{tm4(ACTB-tdTomato,-EGFP)Luo}$/J (mTmG)	The Jackson Laboratory	RRID:IMSR_JAX:007676
Oligonucleotides		
Primers for qRT-PCR: see the Supplemental Table 2	Integrated DNA Technologies	N/A
Software and algorithms		
GraphPad Prism	GraphPad Software	https://www.graphpad.com/scientific-software/prism/; RRID:SCR_002798
DESeq2	Bioconductor	https://bioconductor.org/packages/release/bioc/html/DESeq2.html; RRID:SCR_015687
Splice-aware STAR aligner	Software tools for Academics and Researchers	http://code.google.com/p/rna-star/; RRID:SCR_004463
ImageJ	ImageJ	https://imagej.net/; RRID:SCR_003070

REAGENT or RESOURCE	SOURCE	IDENTIFIER
Zen	Zeiss Group International	http://www.zeiss.com/microscopy/en_us/products/microscope-software/zen.html#introduction; RRID:SCR_013672
Adobe Photoshop CC	Adobe	https://www.adobe.com/products/photoshop.html; RRID:SCR_014199
FlowJo 10.7.1	Tree Star	https://www.flowjo.com/solutions/flowjo; RRID:SCR_008520
Imaris v9.7	Andor Technology PLC	http://www.bitplane.com/imaris/imaris; RRID:SCR_007370
Other		